PERFORMANCE EVALUATION OF EFFECTIVE SENSORS TO ACHIEVE RELIABLE FLARE ALTITUDE FOR FIXED WING UAV

MUHAMMAD MAHFUZUR RAHMAN (SN. 1016160001 P)

A Thesis Submitted in Partial Fulfillment of the Requirements for the
Degree of Master of science in
Electrical, Electronic and Communication Engineering

DEPARTMENT OF
ELECTRICAL, ELECTRONIC AND COMMUNICATION ENGINEERING
MILITARY INSTITUTE OF SCIENCE AND TECHNOLOGY
DHAKA, BANGLADESH

MARCH 2023

PERFORMANCE EVALUATION OF EFFECTIVE SENSORS TO ACHIEVE RELIABLE FLARE ALTITUDE FOR FIXED WING UAV

M. Sc Engineering Thesis

By

MUHAMMAD MAHFUZUR RAHMAN (SN. 1016160001 P)

Approved as to style and content by the Board of Examination on 28 March 2023

Dr Md Hossam-E-Haider Professor Department of EECE MIST, Dhaka	Chairman (Supervisor) Board of Examination
Dr Pran Kanai Saha Professor Department of EEE BUET, Dhaka	Member (External) Board of Examination
Wg Cdr Toyobur Rahman Instructor Class A Department of EECE MIST, Dhaka	Member Board of Examination
Brig Gen Md Mahfuzul Karim Majumder Dean Faculty of ECE MIST, Dhaka	Member (Ex-officio)

Department of EECE, MIST, DHAKA

PERFORMANCE EVALUATION OF EFFECTIVE SENSORS TO ACHIEVE RELIABLE FLARE ALTITUDE FOR FIXED WING UAV

DECLARATION

I hereby declare that the study reported in this thesis entitled as above is my own original work and has not been submitted before anywhere for any degree or other purposes. Further I certify that the intellectual content of this thesis is the product of my own work and that all the assistance received in preparing this thesis and sources have been acknowledged and/or cited in the reference Section.

_____

Muhammad Mahfuzur Rahman

PERFORMANCE EVALUATION OF EFFECTIVE SENSORS TO ACHIEVE RELIABLE FLARE ALTITUDE FOR FIXED WING UAV

A Thesis

By

MUHAMMAD MAHFUZUR RAHMAN

DEDICATION

To my parents and family.

ACKNOWLEDGMENT

Foremost, I would like to express my sincere gratitude to my supervisor, Prof Md Hossam-E-Haider of the Department of EECE, MIST for the useful comments, remarks and engagement through the learning process of this master thesis. I thank him from the core of my heart for his unwavering support and invaluable guidance since I started working with him. It had been a great privilege and honor to work and study under his direct supervision. The door to his office was always open whenever I had a question about my research or writing. He has taught me the methodology to carry out the research and to present the research works as clearly as possible.

Besides, this thesis would not have been completed without the guidance and the help of a few other people. I must express my profound gratitude to Wing Commander Toyobur Rahman, PhD, Major Md Aminul Islam, PhD, EME. I also offer my sincere appreciation for the learning opportunities provided by MIST, and acknowledge the support provided by all the MIST office staffs.

Finally, but not least, I owe a huge debt of gratitude to my parents, their love and confidence in me have encouraged me to go ahead in my study and career. Most importantly, I wish to thank my family for their love, understanding, inspiration, prayers and continuing support to complete this research work. Thanks to the Almighty, for keeping me physically and mentally well throughout my research work.

_____

Muhammad Mahfuzur Rahman

ABSTRACT

Unmanned aerial vehicles (UAVs), also known as drones, have gained popularity and significant attention in different disciplines of military and civilian services due to their versatility, lower cost and ease of deployment. Just like any other fixed wing aircraft, landing phase of fixed wing UAV is the most critical and challenging phase of flying. GPS has been widely used as the primary navigation sensor for UAVs but the accuracy of GPS, without any form of augmentation, is not enough for autonomous landing where precise height estimation is mandatory for safe landing. Although, most of the fixed wing UAVs are equipped with autonomous landing system, still it is recommended to put a human pilot in the loop for a safer landing. In addition to GNSS and INS, state of the art fixed wing military UAVs are aided by ground-based landing radars for safe autonomous landing. Ground based landing radars are expensive as well as restrict operation of UAVs to specific runways equipped with radars. Now a days, RTK GPS receivers are getting cheaper and more accurate. Cheaper laser distance measuring sensor like LIDAR can also be used for precise altitude measurement. In this research work, altitude estimating performances of GPS, RTK GPS and LIDAR have been compared using Software in The Loop (SITL) simulation to find out which sensor works best as reliable flare altitude estimating sensor for fixed wing UAV. The findings of simulation were further consolidated by developing a test setup and carrying out test flights. Simulation and test flight results show the potentials of using cost effective sensors like LIDAR sensor and RTK GPS as landing aid during the flare phase of landing for fixed wing UAV.

TABLE OF CONTENTS

LIST OF FIGURES

LIST OF TABLES

LIST OF ABBREVIATIONS

AGL	Above Ground Level
AHRS	Attitude and Heading Reference System
ANOVA	Analysis of Variance
AUVSI	Association for Uncrewed Vehicle Systems International
CEP	Circular Error Probable
DF	Direction Finder
DJI	Shenzhen DJI Sciences and Technologies Ltd, a Chinese drone manufacturer
EKF	Extended Kalman Filter
FAA	Federal Aviation Authority
FDM	Flight Dynamics Model
FRP	Fiber reinforced polymers
GCS	Ground Control Station
GNSS	Global Navigation Satellite System
GPS	Global Positioning System
ILS	Instrument Landing System
INS	Inertial Navigation System
ISM	Industrial, Scientific, and Medical
LIDAR	Light Detection and Ranging
LiPo	Lithium-Ion Polymer
MAVLINK	Micro Air Vehicle Link
MLS	Microwave Landing System
NTRIP	Networked Transport of RTCM via Internet Protocol
QFE	Pressure above airfield in aviation terminology

QNH	Pressure at the Mean Sea Level in aviation terminology
RTCM	Radio Technical Commission for Maritime Services
RTK	Real Time Kinematics
SITL	Software in The Loop
SNR	Signal to Noise Ratio
SONAR	Sound Navigation Ranging
SPI	Serial Peripheral Interface
UAV	Unmanned aerial vehicle
UART	Universal Asynchronous Receiver / Transmitter
VS0	Stall Speed at Landing Setting

LIST OF SYMBOLS

VS0	Stalling Speed at Landing Configuration
c	Speed of light
$\triangle t_i$	Signal travel time for satellite i,
(x_i, y_i, z_i)	Coordinates for satellite i
A and B	Signal's amplitude
f	Signal's frequency
d	Distance travelled by the signal
λ	Wavelength of the signal
∅rec	Signal phase measured at the receiver
$\emptyset_{stn,i}$	Measured signal phase of satellite i
N_i	Unknown integer ambiguity for satellite i
$\epsilon_{\emptyset}$	Unknown hardware noise and multipath etc
I_i	Unknown ionospheric error for satellite i
T_i	Unknown tropospheric error for satellite i
$b_{sat,i}$, b_{stn}	Unknown clock biases of satellite i and station
ρ_i	Known distance of satellite
H	Measured altitude
T_H	Lower limit of atmospheric temperature
P_H	Lower limit pressure value,
U	Vertical temperature gradient,
Tb	Sea level temperature at standard atmosphere,
P_b	Sea level static pressure,
R	Special gas constant = 287.05287m2/(K0/s2)

v_g	Group velocity of the pulse,
T_t	Travel time of the pulse
t_r	Transmit rise time
p	PRF of the signal
$\Delta\theta$	Angular beamwidth of the system
H	Range (height)
F_{Comd}	Commanded Flare Altitude

CHAPTER 1
INTRODUCTION

1.1 Introduction

In recent decades, Unmanned Aerial Vehicles (UAVs) have enjoyed an exponential growth of usage in military and civilian applications. Accordingly, UAVs have gone through tremendous improvements in terms of their structure, working methodology, flying features and navigation control. In addition to military applications, UAVs are highly utilized in a wide range of services such as photography, path planning, search and rescue, inspection of power lines and civil constructions, etc due to their ubiquity, ease of use, lower training requirement and overall cost effectiveness. An aerial survey would have cost several flight hours of manned aircraft before the age of UAVs, now all it takes a low-cost drone to take survey of an area with a fraction of cost of manned aircraft flight hour. In all recent warfare, UAVs has dominated the war field for its ubiquity, rapid deployment capability, lower training requirements and overall cost effectiveness. Accordingly, significant amount of budget is dedicated to UAVs. For example, AUVSI reports [1] Department of Defense, USA plans to invest more than $2.6 billion in unmanned systems in 2023, with at least 29 programs fully dedicated to Unmanned Aerial System (UAS). The UAV market is poised to grow by $32.41 bn during 2022-2026 [2].

Size and shape of UAVs vary largely due to their diversified application and purpose. An UAV can be as small as DJI Mini 3 with all up weight of 249 gram to large military UAV like Global Hawk weighing 14,628 kg. UAVs can be broadly categorized into two categories like fixed wing and rotary wing. Rotary wing UAVs like quadcopter, octocopter etc. give the flexibility of easy launch and recovery but suffer from shorted endurance and low payload. Large fixed wing UAVs require runway for take-off and landing but can provide heavy payload and longer endurance and are better suited for military application.

With advancement of technology the UAVs are getting higher degree of autonomy. Advanced UAVs are now capable of fully autonomous flight including take-off and landing. But as like other manned aircraft, landing phase of UAV remains as the most challenging and critical phase of flight [3]. This thesis is aimed at investigating

effective sensors which can be used as landing aid for fixed wing UAV during autonomous landing.

GPS has been widely used as the primary navigation sensor for UAVs but the accuracy of GPS, without any form of augmentation, is not enough for autonomous landing [4] [5] where precise height estimation is mandatory for safe landing. Although, most of the fixed wing UAVs are equipped with autonomous landing system, it is still recommended to put a human pilot in the loop for a safer landing. In addition to GNSS and INS, state of the art fixed wing military UAVs are aided by ground-based landing systems like Landing radars, radar altimeter, ILS, MLS, Radio Direction Finder (DF) or Laser based DF for safe autonomous landing [6] [7]. Ground based landing systems restricts operation of fixed wing UAVs to specific runways equipped with radars and equipping every potential runway with landing radar is costly. As the key to a good landing is precise height estimation at the terminal phase of flight [3] height estimating sensors like GPS [4] [8], RTK GPS [3] [9], Sonar sensors [10] and LIDAR [11] worth investigating. Performance analysis of those sensors might provide a cheaper and reliable alternative as landing aid of fixed wing UAV.

1.2 Literature Review

Ahmed, et al. identified, research paper related fixed wing UAV is significantly lower than the other popular types like quadcopter, octocopter, hexacopter etc [12].

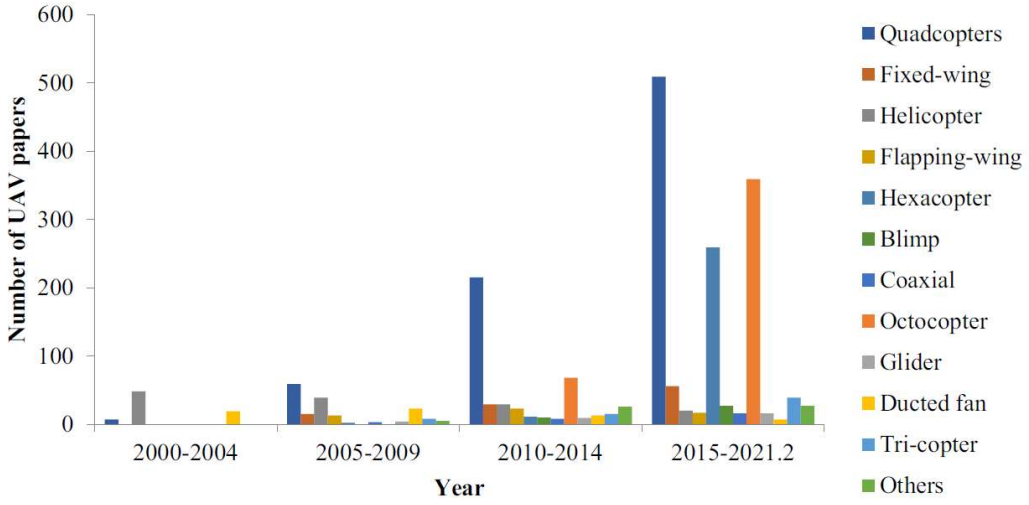

Fig 1.1: Research conducted on various types of UAV

Lack of testing facility i.e., requirement of runway is the main reason for a smaller number of research on fixed wing UAV. However, for this research a good number of papers have been consulted. Notable of them are as following:

Skulstad, et al conducted research using single frequency RTK GPS as navigational sensor in a fixed wing UAV for net recovery system [3]. In that research A relatively simple system for autonomous net recovery of small fixed-wing UAVs has been designed and field tested.

Fig 1.2: Test UAV for the Net Recovery System

The system is based on low-cost hardware such as single frequency GPS receivers, broadband radio communication, and open-source software for flight control and RTK computations. The flight tests with a prototype implementation demonstrate successful UAV recovery with the UAV hitting the center of the landing net with less than 1 m error horizontally and vertically.

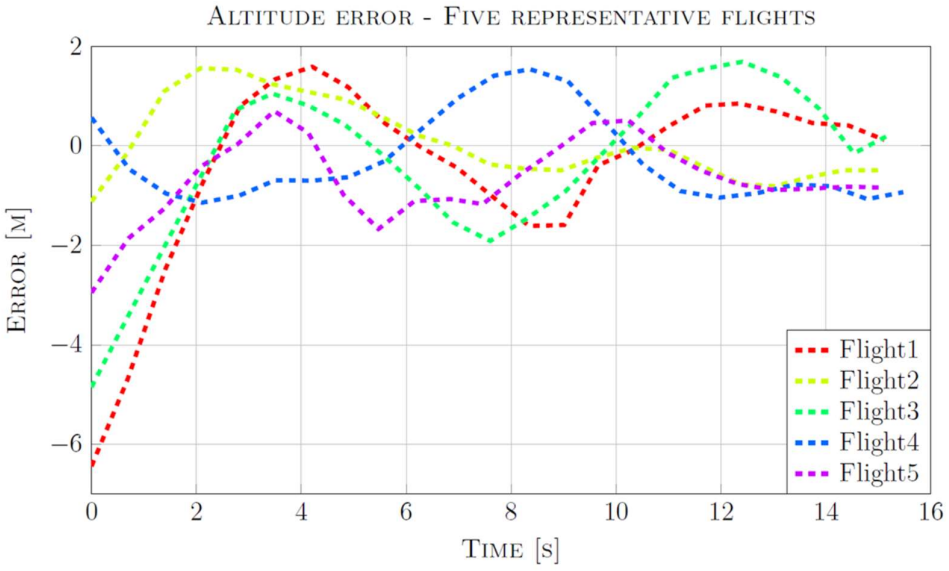

Fig 1.3: Vertical Error obtained by using RTK GPS

Yuxi, et al proposed an algorithm for vision based autonomous drone landing using GPS and image processing [4]. Since the applicable range of GPS is known (> 1.5 m), image processing was used at the terminal phase of landing. For GPS and image processing navigation, they both return a direction and distance that the UAV needs to move toward the landmark, regardless of whether the result is accurate or not. Therefore, authors proposed different weights to different navigation results. This is a bi-objective optimization problem. Since GPS and image processing targets do not reach the optimal conditions at the same time, an algorithm was proposed that comprehensively consider both, that is, to determine their respective weights.

The developed algorithm was tested on an Anotech Exploiter quadrotor UAV. In terms of image processing, the practicality of the algorithm has been verified by testing numerous pictures. The results show that the algorithm does noise removal very well and recognize triangles. Through the experimental verification, the comprehensive bi-objective optimization model can indeed combine the results of GPS and image processing to obtain comprehensive navigation information, and finally guide the UAV to land on the landmark.

Hügler, et al conducted a study using 122 GHz monostatic radar for autonomous landing of hexacopter [7]. The authors recocnised that for automated landing of UAVs and hovering in close proximity to ground, the precise altitude AGL must be known. For all measurements a test carrier based on a DJI Matrice 600 Pro hexacopter was used.

Fig 1.4: Matrice 600 Hexacopter used as test platform for 122 GHz monostatic radar

Authors presented that with the 122 GHz monostatic radar sensor, high bandwidth can be achieved in order to obtain range resolution in the single digit cm-range and thus obstacles or unsuitable terrain for landing can be detected. With 5 GHz bandwidth the complete takeoff starting with the UAV being on ground and continuing the ascend of the UAV can be precisely captured. The study concluded that 122 GHz radar altimeter with 5 GHz bandwidth satisfies all requirements for the close-range performance.

Kang, et al performed precision landing flight test of a tilt-rotor UAV called the TR-60M on shipboard and motion platforms [9]. The ship moved at 10 kt speed on the sea in a sea-state 2 condition, and the motion platform also moved at 10 kt speed between the edges of a runway while simulated with sea-state 2 motion during the flight test. All flight tests were performed using the automatic takeoff, hover, and landing function of TR-60M based on the relative navigation. RTK GPS was the main positional sensor for the UAV. A total of 11 and 10 sorties of automatic takeoff and landing were performed to evaluate the landing accuracy on the running motion platform and shipboard, respectively. The accuracy of the precision landing test satisfied the requirements of shipboard landing in the sea-state 2 condition.

Fig 1.5: Recovery of Tilt Rotor Platform on moving ship using RTK GPS

During 11 trials of automatic landing on the motion platform at 10 kt speed while simulating sea-state 2, the CEP value was calculated as 0.9039 m which satisfied the requirement of CEP<2 m. The mean value and standard deviations were 0.9874 m and 0.3399 m, respectively, and the mean value was slightly higher than the CEP value. The Circular Error Probable (CEP) of 10 flight sorties that was obtained by the authors was 1.132 m. The authors noted, CEP of the shipboard landing was 1.132, whereas the value was 0.904 in the motion platform case. Those accuracies of the flight test results were significantly worse than those of the simulation and were 0.71±0.28 m with an RMS error in the sea-state 0 condition. The difference of landing accuracy between the simulation and flight test results was mainly a result of the effect of air wakes, which were more severe than expected.

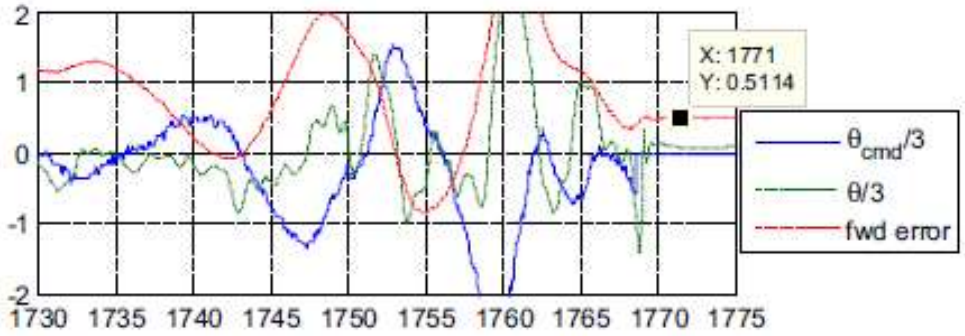

Fig 1.6: Positional error by RTK GPS for a tilt rotor UAV

Jantawong et al presented an automatic landing scheme for a small fixed-wing aircraft [8]. Since visual servoing usually suffers from bad light condition, the authors instead proposed a GPS based approach. On-board GPS device along with other sensors would track the designed flight path which has been determined from the computed coordinates of the final approach and flare legs. These two coordinates had been determined according to headwind and crosswind speeds so that the heading of the aircraft would align with the heading of the runway. The height of the aircraft was computed based on differential pressure between the on-board barometric sensor and ground barometric sensor. The proposed automated landing system was tested using an UAV having 1.7 m. wing span with 2 stroke engine 10.63 cc. (roughly 1.73 hp at 16,000 rpm). The max flight time was 60 minutes with 950 cc nitro fuel tank. The total weight including fuel is 3.5 kg. In terms of aircraft's performance, the maximum cruise speed was at 17 m/s, touch seed at 11 m/s, maximum sink rate is 4 m/s and the maximum bank turn radius is 100 m. Fig. 1.7 shows the fixed-wing aircraft that was used.

Fig 1.7: Fixed wing aircraft used by Jantawong et al [8]

The field test showed that approach started at 730 m. away from the touch point. Then, the aircraft started to lower its altitude according to the reference trajectory with the sink rate of 0.33 m/s. Even though the aircraft was above the reference trajectory most of the time, the error at touch position is 4.3 m.

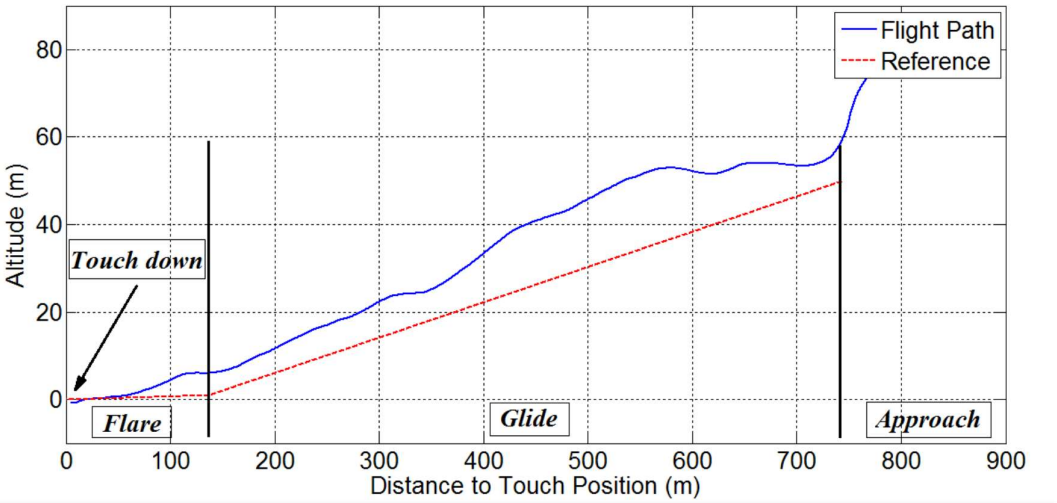

Fig 1.8: Experimental result of automatic landing by Jantawong et al [8]

1.3 Research Motivation

The research is motivated by two factors. First of all, to investigate alternative altitude estimating sensors to facilitate autonomous landing of UAV. If the real-life accuracy of altitude estimating sensors can be tested, it could help the UAV designers to integrate those sensors in their design. Traditionally, aircrafts use barometer to measure the altitude but barometers require calibration and QNH/QFE setting before each flight or sometimes during the flight. Even with proper setting, barometer suffers from inaccuracies in tens of meters. GPS also suffers from inaccuracy in altitude estimation by magnitude of few meters. But for autonomous landing of UAV where precise altitude estimation is mandatory, there is a strong requirement of precise altitude estimating sensors. Precision in altitude measurement should be the main criteria for these sensors. Unlike the unlimited range of barometer or GPS, these sensors could be of shorter range but should have enough range to be used during the landing phase only. This is the main motivation for this thesis to investigate the performance of altitude estimating sensors which could be used during landing phase of autonomous UAVs.

The second motivation for this thesis is to reduce cost of UAV system. There is a high demand of low-cost UAV in the armed forces as well as in the civilian market. If some low-cost sensors can be explored which can be used as landing aid of UAV while

not compromising the precision and safety of the system, it would reduce overall cost of UAV that can perform autonomous landing safely.

1.4 Research Objectives

In light of reasons mentioned in Section 1.1 and gap in research mentioned in section 1.2 as well as motivation mentioned in section 1.3, the objective of this investigation is to find the accurate flare altitude using various altitude sensors like Barometric altimeter, GPS, RTK GPS, Laser Range Finder and SONAR sensor and find out the best possible sensor for perfect and reliable flare altitude through simulation and test flight. To achieve the final objective, the following specific objectives have been set:

a) To investigate the current state of accuracy of cost-effective sensors by analyzing literatures to determine the feasibility of utilizing them during landing phase of fixed wing UAV.
b) To develop a simulation setup to measure the accuracy of flare altitude estimation using Standard GPS, RTK GPS and LIDAR in a fixed wing UAV.
c) To develop a test set up and measure the accuracy of flare altitude estimation during flight test using same set of sensors.
d) To evaluate, compare and analyze the accuracy obtained through test flight and simulation.

With successful attainment of the specific objectives, the expected outcome of the research is to find out the accuracy of flare altitude estimation during the landing phase of the fixed wing UAV using low-cost sensors.

1.5 Organization of the Research

The remainder of this thesis is organized as follows.

Chapter 2 discusses the background of the research from different literatures to find out feasible sensors that can be used as landing aid for fixed wing UAV. Each

sensor is discussed with their principle of operation, limitations, cost and theoretical accuracy that can be achieved from these sensors.

Chapter 3 discusses a simulation setup for testing these sensors as flare altitude estimator. This chapter also discusses a test setup for testing feasible sensors in real time flight test.

Chapter 4 presents and analyzes the result found in simulation and real time test flights and compares the results with contemporary literature.

Chapter 5 presents the conclusion of the thesis with summary of the result, significance of the research and future works.

CHAPTER 2
BACKGROUND

2.1 Introduction

This chapter discusses about the phases of landing specially highlighting the importance of precise flare altitude estimation during the landing of autonomous fixed wing UAV. As this thesis aims to analyze the performance of different flare altitude estimating sensors, subsequent sections of this chapter elaborately discuss different altitude estimating sensors, their working principle and their theoretical accuracy. Strength and weakness of each sensor as well as their cost have also been discussed.

After that, a comparative study on performance of sensors have been prepared. Basing on the comparative study of these sensors this chapter explores the feasibility of using those sensors as altitude estimating sensors in autonomous UAV landing.

2.2 Phases of Landing

The landing of any fixed wing aircraft consists of five phases. They are: Base leg, the final approach, flare, touch down and after landing rolling [13]. Following sub paragraphs discusses them briefly:

2.2.1 Base Leg

The placement of the base leg is one of the more important judgments made by the pilot in any landing approach. The pilot must accurately judge the altitude and distance from which a gradual, stabilized descent results in landing at the desired spot. The distance depends on the altitude of the base leg. After turning onto the base leg, start the descent with reduced power and airspeed of approximately 1.4 VS0, which is the stalling speed with power off, landing gear and flaps down ie landing configuration. For example, if VS0 is 60 kt, the speed should be 1.4 times 60 or 84 kt. The base leg is continued to the point where a medium to shallow-banked turn aligns the airplane’s path directly with the centerline of the landing runway.

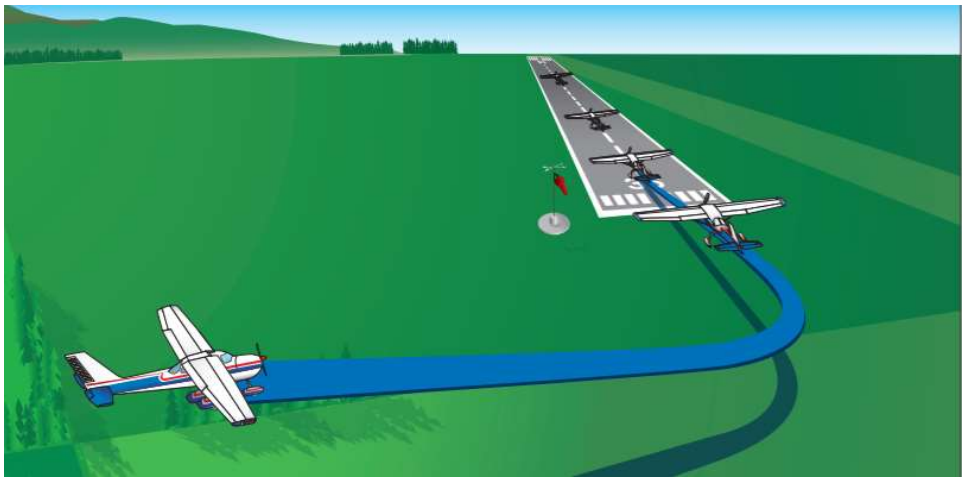

Fig 2.1: Base Leg and Final Approach

2.2.2 The Final Approach

After the base-to-final approach turn is completed, the longitudinal axis of the airplane is aligned with the centerline of the runway or landing surface so that drift (if any) is recognized immediately. On a normal approach, with no wind drift, the longitudinal axis is kept aligned with the runway centerline throughout the approach and landing. After aligning the airplane with the runway centerline, the final flap setting is completed and the pitch attitude adjusted as required for the desired rate of descent.

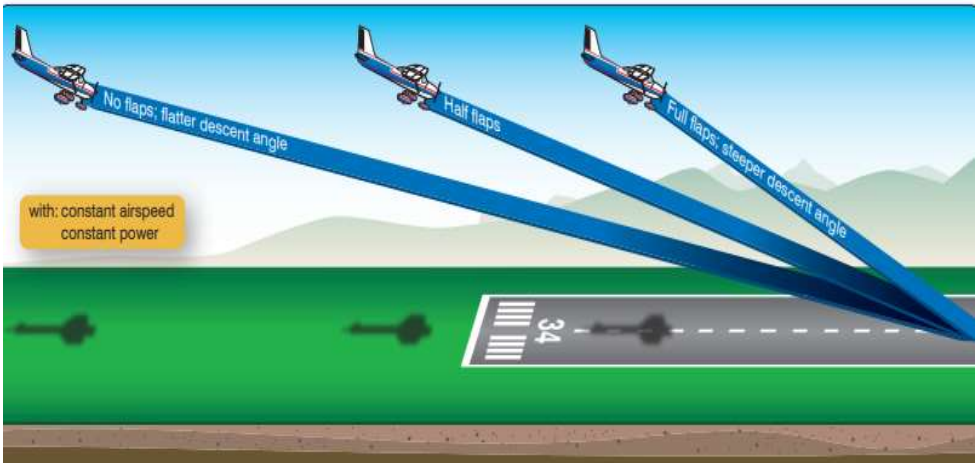

Fig 2.2: Final approach and effect of Flaps

2.2.3 The Flare

The round out is a slow, smooth transition from a normal approach attitude to a landing attitude, gradually rounding out the flightpath to one that is parallel with, and within a very few inches above, the runway. When the airplane, in a normal descent, approaches within what appears to be 10 ft to 20 ft above the ground, the round out or flare is started. This is a continuous process until the airplane touches down on the ground.

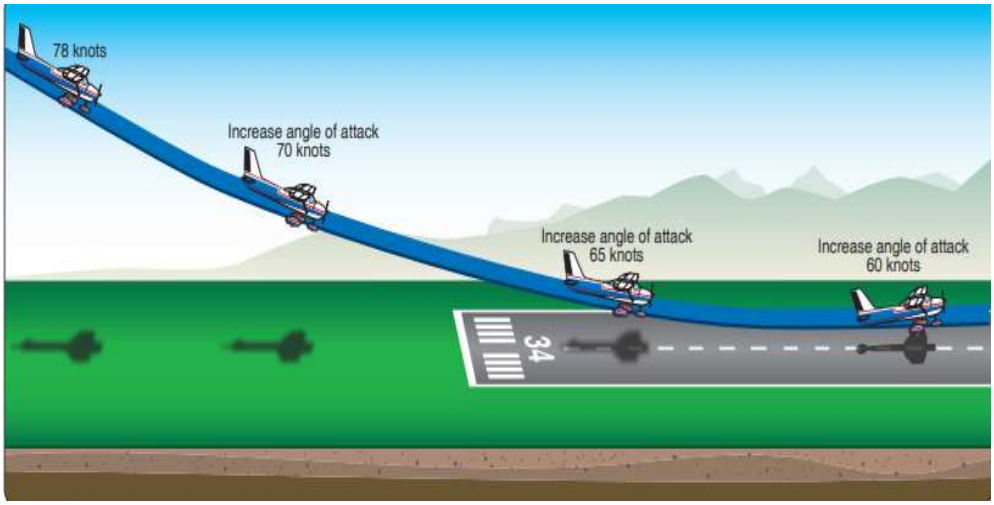

Fig 2.3: Flare process for smooth touchdown

2.2.4 Touchdown

Touchdown is the gentle settling of the airplane onto the landing surface. The round out and touchdown are normally made with the engine idling and the airplane at minimum controllable airspeed so that the airplane touches down on the main gear at approximately stalling speed.

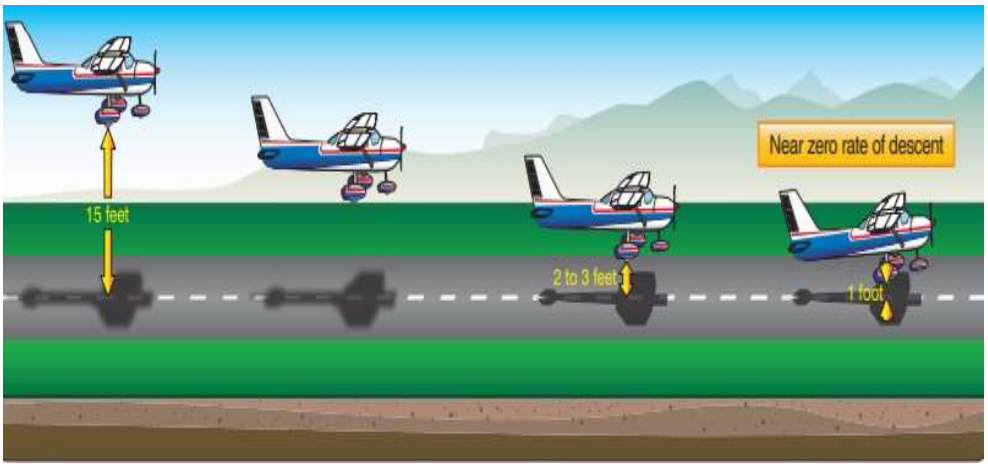

Fig 2.4: Properly executed Touchdown results in almost zero rate of descent

2.2.5 After Landing Roll

The landing process must never be considered complete until the airplane decelerates to the normal taxi speed during the landing roll or has been brought to a complete stop when clear of the landing area.

2.3 Flare Altitude and its significance

The optimum altitude for flare depends on the aerodynamic performance of the specific aircraft and it is normally defined by the manufacturer of the aircraft. In most of the fixed wing transport planes flaring at the altitude of 10-15 ft (3-5 m) would be enough for smooth landing. Larger planes require higher flare altitude. Smaller planes like UAVs might require to flare at 1-3 m for smooth landing.

Execution of flare at right altitude is critical for smooth landing. Flaring at too high altitude will result in 'floating' the aircraft for longer distance and might overshoot the runway. On the other hand, flaring at lower altitude might result in a rough landing and will increase the probability of hitting the nose landing gear and in worst case it might lead to crash landing.

2.4 Flare Altitude Estimating Sensors

In case of autonomous landing of UAV, as there is no pilot on board, the autopilot has to rely on altitude estimating sensors to determine the perfect altitude of flare. The following subsections discusses about various altitude estimating sensors

2.4.1 RTK GPS

In most of the autonomous UAVs, GPS (or GNSS) receiver has been extensively used as the primary sensor for navigation. The mathematical principle behind GPS positioning is [14]:

$$c\Delta t_i = \sqrt{\{(x - x_i)^2 + (y - y_i)^2 + (z - z_i)^2\}} \quad (2.1)$$

Where:

c = speed of light

Δt_i = Signal travel time for satellite *i*

(x, y, z) = GPS receiver coordinates;

the variables (x_i, y_i, z_i) = Coordinates for satellite *i*

Equation (1) has 3 variables, they are latitude, longitude and altitude. So, if the ephemeris of 3 satellites are known and signal travel time from satellite to user receiver is known, it is possible to calculate the position of the receiver. As the speed of light is 300,000km/s; 1ms error in calculation will yield in receiver's position offset by 300 km [14]. GPS suffers from different types of errors like satellite and receiver clock error, multipath error, ionospheric error, ephemeris error. Standalone GPS without any form of augmentation will lead to an error of 30 cm to 5 m [15] which is not suitable for autonomous UAV landing.

RTK is a real time GPS augmentation technique, originated in 1990s, which can improve precision substantially. A typically RTK system consists of a RTK base station, a RTK rover and communication channel to transmit correction information to the rover. In this method, range is determined by counting the number of carrier cycles that has passed for the signal to reach from satellite to receiver plus the phase (fraction of

wavelength) and then multiplying number of cycles with the wavelength of the carrier. It still contains errors like satellite and receiver clock error, multipath error, ionospheric error, ephemeris error which can be resolved by transmitting same set of measurement to the rover by the communication channel.

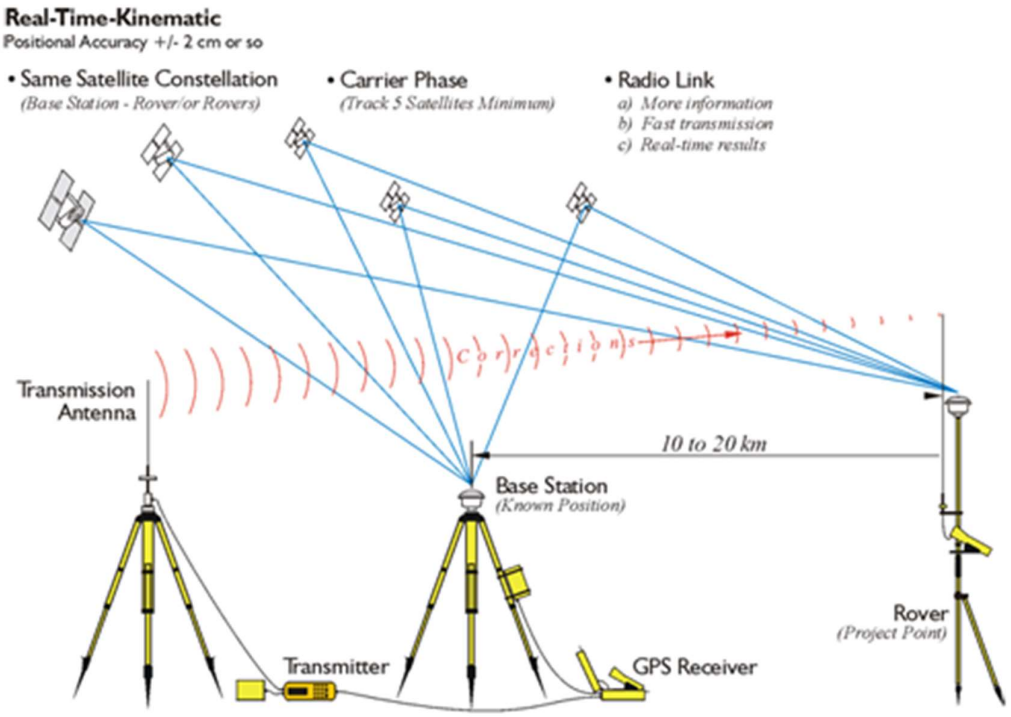

Fig 2.5: RTK GPS architecture

Then, by subtracting the measured phases from the vehicle/rover and a fixed-position base station, almost all errors are eliminated except the phase's integer ambiguity [16] [17]. A complicated process is required to calculate the number of whole cycles which is known as carrier ambiguity resolution. Different types of ambiguity resolution techniques like float and fix are available. Float resolution requires minimum 4 common satellites between base and rover whereas fixed resolution requires minimum 5 common satellites which can provide accuracy up to 20 cm and 2 cm respectively [18]. Equation 2.2 and 2.3 represent two sinusoidal signals generated from a transmitter at unknown distance and another is locally generated [16]:

$$f_{rec}\ (t, d) = \text{Acos}\ (2\pi \text{ft} + \frac{2\pi}{\lambda}\ \text{d}) \tag{2.2}$$

$$f_{local}(t) = \text{Bcos}(2\pi f t) \tag{2.3}$$

where,

A and B = signal's amplitude

f = signal's frequency

d = distance travelled by the signal

λ = wavelength of the signal

Multiplication of equation (2) and (3) yields in a sum of cosines where the second term depends only on the phase, which is subject to the distance between receiver and transmitter.

$$f_{rec} \times f_{local} = \frac{AB}{2}\left[\cos\left(4\pi f t + \frac{2\pi}{\lambda} d\right) + \cos\left(\frac{2\pi}{\lambda} d\right)\right] \tag{2.4}$$

However, the distance d can be expressed as a function of the signal wavelength; therefore:

$$d = N\lambda + \lambda \frac{\phi_{rec}}{2\pi} \rightarrow \cos\left(\frac{2\pi}{\lambda} d\right) = \cos(2N\pi + \phi_{rec}) = \cos(\phi_{rec}) \tag{2.5}$$

where,

N = unknown integer number of wavelengths

$\emptyset_{rec}$ = signal phase measured at the receiver

It is not possible to determine the full distance between the transmitter and the receiver by measuring only the phase. Only the small fractional part of the phase difference can be measured. The unknown N represents the integer ambiguity. The signal phase measured at the base station for each satellite can be modeled as [16].

$$\emptyset_{stn,i} = \frac{2\pi}{\lambda}\left[\rho_i - N_i\lambda + \epsilon_{\emptyset} + I_i - T_i + c\left(b_{sat,i} - b_{stn}\right)\right] \tag{2.6}$$

where,

$$p_i = \sqrt{\left(x_{stn} - x_{sat,i}\right)^2 + \left(y_{stn} - y_{sat,i}\right)^2 + \left(z_{stn} - z_{sat,i}\right)^2} \tag{2.7}$$

where,

$\emptyset_{stn,i}$ = measured signal phase of satellite *i*

N_i = unknown integer ambiguity for satellite *i*

$\epsilon_{\emptyset}$ = unknown hardware noise and multipath etc

I_i = unknown ionospheric error for satellite *i*

T_i = unknown tropospheric error for satellite *i*

c = speed of light

$b_{sat,i}$, b_{stn} = unknown clock biases of satellite *i* and station

If the base station and receiver are assumed to be within 10 km of each other, the ionospheric and tropospheric errors are same and multipath errors and noise can be considered small. Hence, after double difference operation the equation becomes [16]:

$$\triangle \emptyset = \Delta\emptyset_1 - \Delta\emptyset_2 \xrightarrow{yields} \emptyset_{rec.1} - \emptyset_{stn.1} - \emptyset_{rec.2} - \emptyset_{stn.2}$$

$$= \frac{2\pi}{\lambda}\{\rho_{rec.1} - \rho_1 - \rho_{rec.2} + \rho_2 - \lambda(N_{rec.1} - N_1 - N_{rec.2} + N_2)\} \quad (2.8)$$

where,

$\emptyset$ = measured signal phase of satellite

ρ_i = known distance of satellite

N_i = unknown integer ambiguity for *i*

λ = wavelength of the signal

Since all the phases are measured and the distance between station and satellites are known, using pseudo range equation inaccurate distance between satellite and receiver can be determined. Now, equation (8) depends only on resolving integer ambiguity. Different methods can be employed to resolve the integer ambiguity like using pseudo range and calculating ambiguity around float numbers or real valued ambiguity, then finding integer ambiguity around the float value and then calculating accurate receiver position relative to base station using the integer. Once the integer ambiguity is resolver, the RTK receiver goes into fixed mode where it can provide accuracy around 2 cm.

Fig 2.6: Components of RTK GPS
Source: www.cuav.net

For this investigation, a set of RTK base and rover (Model: CUAV C-RTK 9P) has been considered which cost approximately USD 1440.

A study conducted by Suelynn Choy [19] found the accuracy of different augmentation types

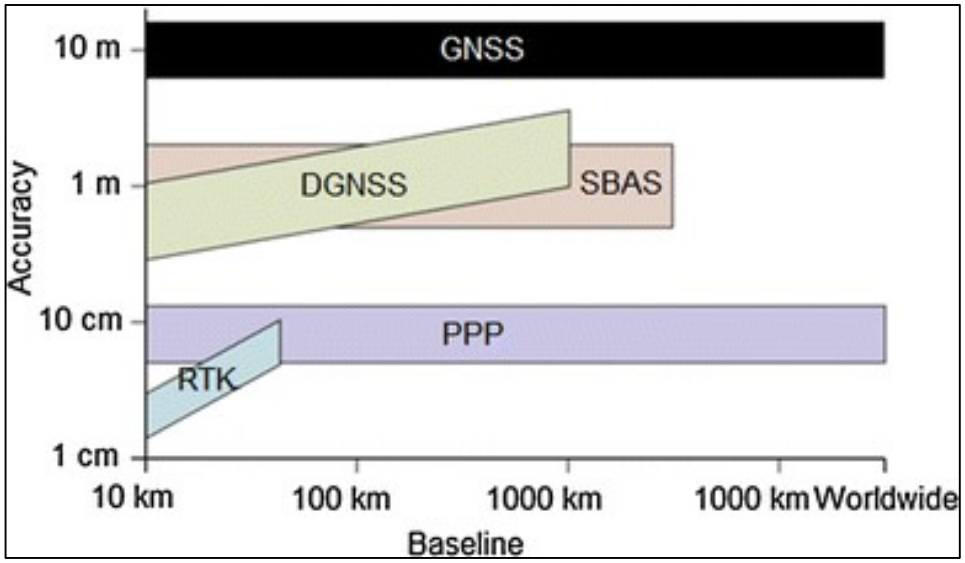

Fig 2.7: Comparison of accuracy of different GPS augmentation techniques

Basing on the study RTK was found to provide the best accuracy in shorter range (typically 0-20 km) from the base station to rover.

2.4.2 Barometric Altimeter

Barometric altimeter is essentially a pressure sensor [20]. As the atmosphere remains relatively constant to earth and doesn't move horizontally or vertically [21], barometric altimeters can convert the change in pressure to altitude information. Altimeters are essential equipment for certification of flight as per Federal Aviation Authority (FAA) [22]. Different types of altimeters are available like bellows type, vibration cylinder pressure type, silicon resonant pressure type, silicon piezoresistive pressure type etc. For this investigation, silicon piezoresistive pressure altimeter has been selected for its lower weight and cost effectiveness. The measured altitude can be expressed as [20]

$$H = \frac{T_b}{U}\left[\left(\frac{P_H}{P_b}\right)^{-U_{R/g}} - 1\right] \tag{2.9}$$

$$H = 11000 + \left(\frac{RT_b}{g}\right)\ln\left(\frac{P_b}{P_H}\right) \tag{2.10}$$

where,

H = measured altitude

T_H = denotes the lower limit of atmospheric temperature

P_H = lower limit of pressure value

U = vertical temperature gradient

T_b = sea level temperature at standard atmosphere

P_b = sea level static pressure

R = special gas constant of air

g = gravity acceleration, 9.80665 m/s^2

For this investigation a silicon piezoresistive solid-state barometric pressure altitude sensor, model MS6511 manufactured by MEAS Switzerland, has been used (cost around USD 20). The sensor is inbuilt with the open-source autopilot model Pixhawk

Cube V5+ manufactured by CUAV. The sensor can measure altitude with 10 cm resolution [23].

2.4.3 LIDAR

LIDAR, also known as Light Detection and Ranging, is an active remote sensing unit that uses artificial light source to measure distance. The laser works in the optical spectrum from 0.25 μm to 11 μm. The laser source emits a pulse which passes through the targeting scattered medium. Following the intersection with target, the echo of the pulse is backscattered towards the receiver of the LIDAR. [24]. As such, range, H can be expressed as [25]

$$H = \frac{v_g T_t}{2} \tag{2.11}$$

Here,

v_g = group velocity of the pulse

T_t = represents travel time of the pulse

Velocity of near infrared and optical radiation differs from speed of light c in vacuum by around 0.03%. As a result, $v_g \approx c$ yields small error.

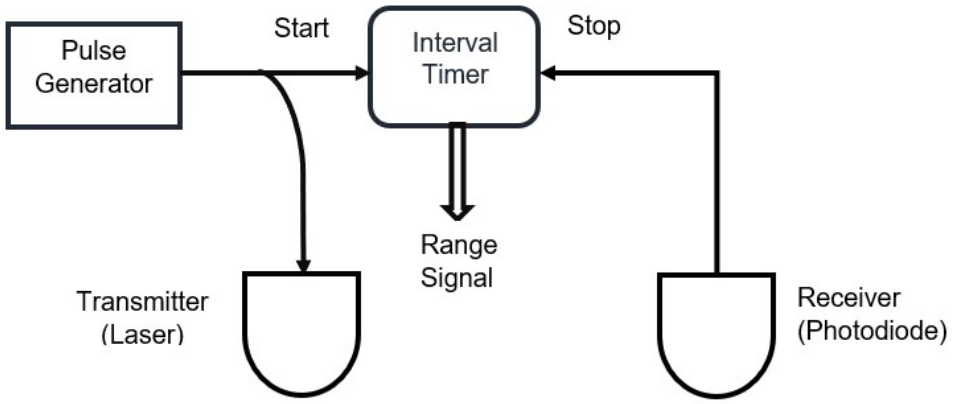

Fig 2.8: Construction of a Laser Range Finder

The range accuracy can be expressed by [25]

$$\Delta H = \frac{v_g t_r}{2S} \sqrt{\left(\frac{v}{pH\Delta\theta}\right)} \tag{12}$$

where,

v = platform velocity

S =SNR

t_r = transmit rise time

p = PRF of the signal

$\Delta\theta$ = angular beamwidth of the system

H = range

Fig 2.9: LIDAR Sensor, Model-LidarLite V3 by Garmin

For the investigation, a LIDAR sensor model Garmin LIDAR Lite V3 was chosen with a measuring range of 40 m which cost around USD 130. The LIDAR has accuracy of +/- 2.5 cm for distances more than 1 m [24].

2.4.4 Sonar

Sonar sensors use soundwave of above 18 kHz, known as ultrasound, to measure the distance of an object. Ultrasonic transmitter sends soundwave greater than 18 kHz in the air where it travels at speed of 344 m/s at 20^0 C and the receiver receives the reflected echo from the targeted object [26]. Sonar sensors do not suffer from lighting conditions, color of the object, transparency of the object. They are also less sensitive to dust. As a result, sonar sensors are a preferred choice in harsh environment and over transparent medium such as water bodies where laser-based sensors are unreliable. Unlike laser-based sensors, sonar sensors provide less range typically around 10 m.

Ultrasonic sensors work with the principle by measuring the time between the transmission pulse (usually few short pulses) and received pulse reflected from the targeted object. Piezoelectric transducers are used as transmitter and receiver which are based on the principle of transferring mechanical waves into electrical signal and vice versa.

The distance between sonar sensor and the measured object can be achieved by using the following equation [27]

$$d = \frac{s}{2} = \left(\frac{vt}{2}\right) \tag{2.13}$$

Where the d denotes the distance between ultrasonic sensor and object, s is the travel distance of ultrasonic wave spread, t is the ultrasonic wave spread time in round trip and v denotes speed of sound in air.

Fig 2.10: Maxbotix Sonar Sensor Model-EZ4

In this investigation, an inexpensive (cost around USD 25) sonar sensor, Model: MaxSonar EZ4 (MB1242) developed by Maxbotix Inc, has been considered. It uses 44 kHz ultrasound wave for measurement and can measure distance up to 765 cm with a resolution of 1mm. It has a blind range of 20 cm [28].

2.5 Comparison of performance

Table 2.1: Comparison of Performance of Altitude Estimating Sensors

Serial no	Sensor	Range	Accuracy	Advantages	Disadvantage
1	RTK GPS	20-30 Km	10 cm	Long Range Does not suffer from visibility condition such as night, fog, cloud	Dependency on base station Required radio link to operate Comparatively expensive
2	Sonar	1 m-7 m	5 cm	Can work over transparent surface such as water Low cost	Low range Influenced by change in temperature
3	LIDAR	40 m	2.5 cm	Long range	Suffers in accuracy over transparent surface such as water Can be affected by fog, low cloud
4	Barometer	Unlimited	15 m	No range limitation Lower cost	Highly affected by change of temperature and air pressure Requires calibration for reliable reading
5	GPS	Unlimited	5 m	Low cost No range limitation	Not enough accuracy for landing

2.6 Selected Sensor for trial

Basing on the performance, accuracy, advantages and disadvantages, it can be deduced that RTK GPS and LIDAR sensor may be the most suitable sensor that can be used as flare altitude estimating sensors for fixed wing UAV. However, for simulation all the sensors were trialed to make a comparison of performance.

2.7 Chapter Summary

His chapter discussed in detailed about different phases of fixed wing aircraft landed. The importance of precise altitude estimation during the flare phase of landing was also discussed elaborately. After that, this chapter introduced different sensors which can be utilized as altitude estimating sensor during flare phase. Working principle as well as their advantage and limitations were also discussed briefly.

Theoretical accuracy of RTK GPS was found around 10 cm, whereas accuracy of LIDAR sensor manufactured by Garmin (model LidarLite V3) was found to be around 2.5 cm. Accuracy of Sonar sensor was found to be around 5 cm. Vertical accuracy of standard GPS, without any form of augmentation varies from within a few meters whereas accuracy of Barometer varies in tens of meters.

Basing on the analysis four sensors; GPS, RTK GPS, Barometer and LIDAR sensor were selected to be used for this investigation as altitude estimating sensor for autonomous landing of fixed wing UAV.

CHAPTER 3
SIMULATION AND TEST FLIGHT SETUP

3.1 Introduction

In chapter 2, importance of precise flare altitude estimation was discussed elaborately. Different low-cost altitude estimating sensors were also discussed along with their accuracy, advantages and disadvantages to select few sensors which might be utilized as flare altitude estimating sensor for fixed wing UAV. In this chapter, a simulation setup has been discussed to simulate the performance of those sensors by installing them, one by one, in a simulated fixed wing UAV.

The subsequent sections discuss a test set up comprising of a small fixed wing UAV and its ground control station to test those sensors by test flights. Scheme for the test flights suitable for testing the sensor performance has also been discussed briefly.

3.2 Simulation Setup

Simulation of a UAV is always less expensive than to test it in real test flight. As the main objective of this thesis is to test the performance of altitude estimating sensors in an UAV, it has been planned to test them in simulation flight as the first step then test them in real test flight. It is expected that simulation would provide close enough results compared to real test flight. Simulation would also provide an opportunity to test the Autopilot configurations, flight planning without the risk of crashing the UAV.

For simulation, an opensource simulator known as ‘Software in the Loop’ (SITL) simulator for drones developed by ArduPilot project has been used. It allows to run UAV autopilot systems on PC directly without using any special hardware. It supports and run on a very wide variety of platforms. In this setup, PC has been used to build and run on the autopilot software. When running the SITL a flight dynamics model in a flight simulator provides the sensor data. This allows the autopilot to be tested on a different types of vehicles like fixed wing plane, single rotor or multirotor platforms etc. In this setup, a simple four channel fixed wing plane has been selected as test platform. [29].

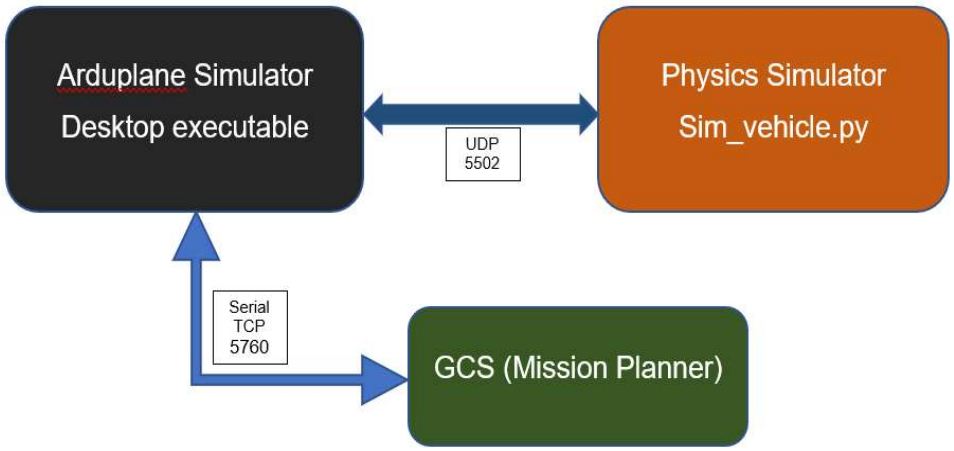

Fig 3.1: Simulation setup

Simulation is implemented by using a Flight Dynamics Model (FDM) of the vehicle to simulate the physics involved with vehicle movement. It receives inputs from a SITL (Software in the Loop) program running the ArduPilot firmware (which are the firmware's servo/motor outputs) and outputs vehicle status, position, velocities, etc. that result from those inputs back to the firmware simulation. Just as sensors would in the real-world case.

Pilot control is implemented either by joystick, dedicated simulation controller box (like Interlink), or by MAVLink commands from a Ground Control Station (GCS) program, like MAVProxy or Mission Planner. For this investigation Mission Planner SITL has been used. The details of the complete process are shown in fig 3.2.

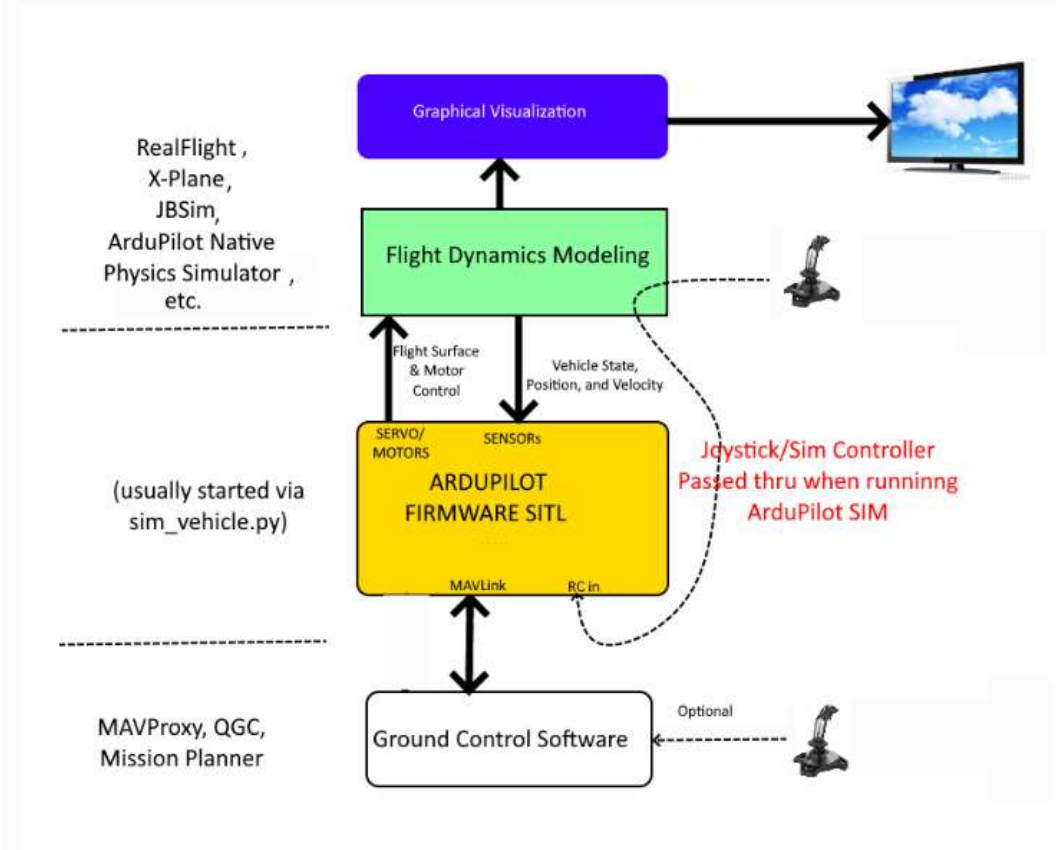

Figure 3.2: Simulation setup architecture

3.2.1 Autopilot configuration

The image below shows the generalized view of the Arduplane architecture. The top-left blue box illustrates how the sensor driver's back-ends are run in a background thread. Raw data from the sensors is collected, converted into standard units and then held within buffers within the driver.

The vehicle code's main thread runs regularly (i.e., 400 Hz for plane) and accesses the latest data available through methods in the driver's front-end. For example, in order to calculate the latest attitude estimate, the Attitude and Heading Reference System (AHRS)/Extended Kalman Filter (EKF) would pull the latest accelerometer, gyro and compass information from the sensor drivers' front-ends.

The image is a slight generalization, for drivers using I^2C or Serial Peripheral Interface (SPI), they must run in the background thread so that the high-rate communication with the sensor does not affect the main loop's performance but for

driver's using a serial interface, it is safe to run in the main thread because the underlying serial driver itself collects data in the background and includes a buffer.

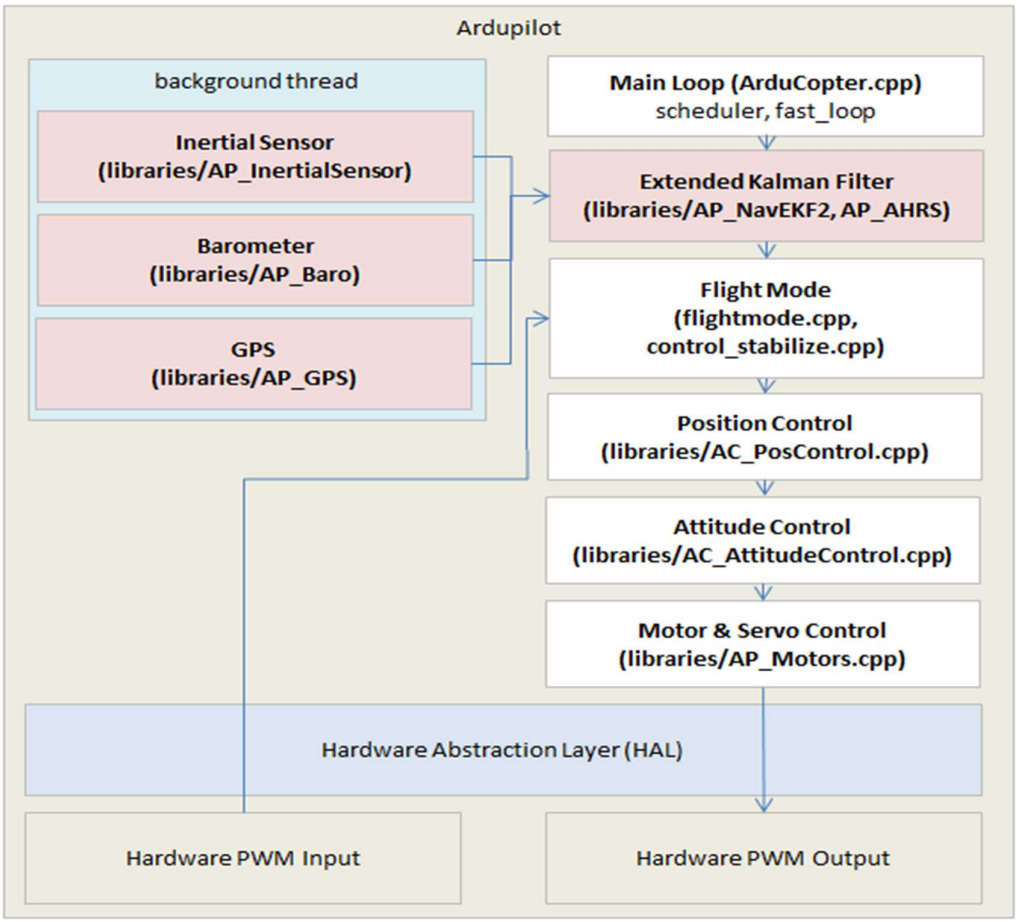

Fig 3.3: Block Diagram of Autopilot working principle

Autopilot configuration has been changed for each sensor simulation. Following is an example to simulate GPS as altitude estimating sensor during landing phase.

param set AHRS_GPS_USE 2 /*GPS for position and Altitude*/

param set EKF2_ALT_SRC 2 /*GPS*/

param set EKF2_RNG_USE_HGT -1 /*Rangefinder Disabled*/

param set EKF2_GPS_TYPE 0 /*GPS 3D Value and Position*/

param set EKF3_RNG_USE_HGT -1 /*Rangefinder Disabled*/

param set EKF3_SRC1_POSXY 3 /*GPS*/

param set EKF3_SRC1_POSZ 3 /*GPS*/

param set RNGFND_LANDING 0 /*Disable*/

param set RNGFND_TYPE 0 /*None*/

param set TECS_LND_SPDWGT 0 /*use throttle to control airspeed not pitch*/

param set LAND_FLARE_ALT 2 /*2m*/

param set LAND_FLARE_SEC 0 /*priority on altitude*/

param set LAND_PITCH_CD 100 /*centidegree*/

param set TECS_LAND_ARSPD default

param set TECS_LAND_SPDWGT 0 /*throttle for speed*/

For setting up a Sonar or LIDAR following parameters are set:

param set SIM_SONAR_SCALE 10

param set RNGFND1_TYPE 1

param set RNGFND1_SCALING 10

param set RNGFND1_PIN 0

param set RNGFND1_MAX_CM 5000

param set RNGFND1_MIN_CM 0

3.2.2 Simulation Mission Profile

Simulation mission profile has been kept simple which follows a circuit with 50m maximum attitude with auto takeoff and landing following standard 3^0 glide slope.

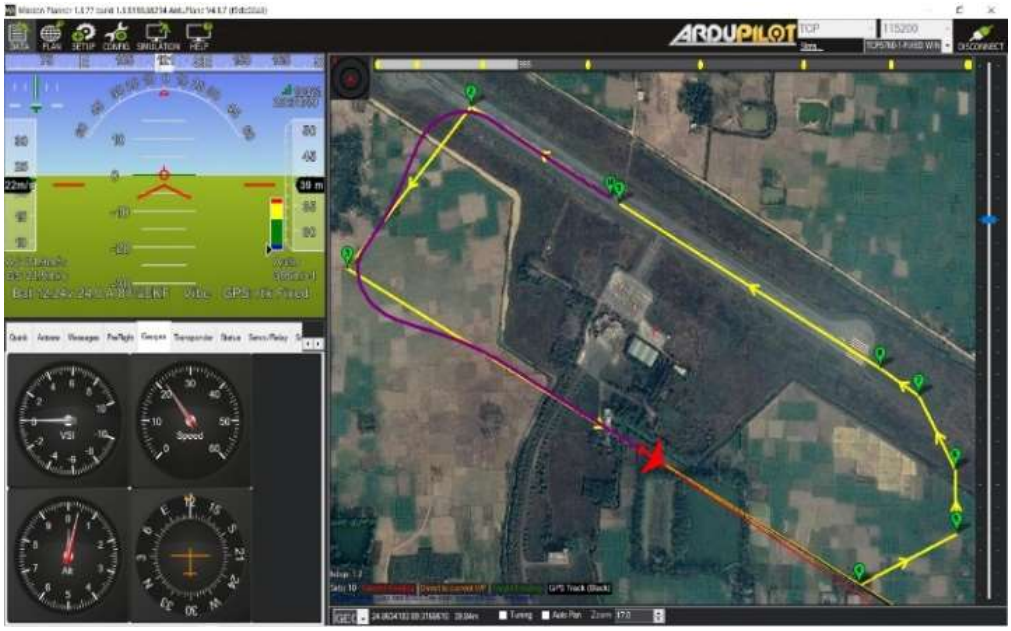

Fig 3.4: Flight path for simulation

All the environmental variables like surface wind, temperature have been kept constant to obtain uniform simulation parameter. All the altitude measuring sensors under test like GPS, RTK GPS, Barometer, Range Finder were simulated one by one. For each sensor 75 simulations were carried out. The commanded altitude for the flare were selected as 1 m, 1.5 m and 2 m. For each commanded flare altitude, 25 simulations were carried out to check if there any variation of accuracy with commanded flare altitude. For all the error measurement, terrain data of Google Earth has been considered as reference.

Table 3.1 shows the number of simulations carried out for each sensor

Table 3.1: Number of Simulation for each sensor

Case	Sensor Used	Commanded Flare Altitude	Number of Simulation
1.	GPS	1 m	25
2.	GPS	1.5 m	25
3.	GPS	2 m	25
4.	RTK GPS	1 m	25
5.	RTK GPS	1.5 m	25
6.	RTK GPS	2 m	25
7.	Barometer	1 m	25
8.	Barometer	1.5 m	25
9.	Barometer	2 m	25
10.	Range Finder (LIDAR)	1 m	25
11.	Range Finder (LIDAR)	1.5 m	25
12.	Range Finder (LIDAR)	2 m	25

3.3 Test Flight Setup

To test the concept a simple fixed wing Radio Controlled aircraft was designed. The aircraft was equipped with open source Ardupilot hardware and firmware which provided autonomy for the plane. For Realtime mission control, configuration and measurement. the plane is connected to a ground control station software running in a laptop by duplex datalink.

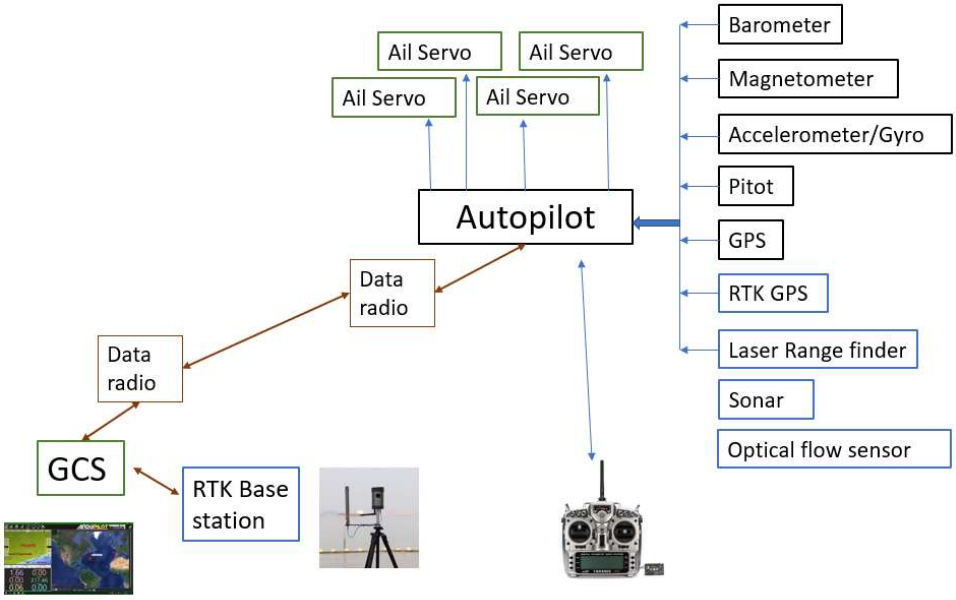

Fig 3.5: Test Flight Setup

3.3.1 UAV design

A simple stable airframe was build using Fiber Reinforced Polymer (FRP) and balsa wood. The UAV was powered by a 4200 mAH 6 cell lithium-ion polymer (LiPo) battery that can provide approximately 15 minutes flight time. The airframe was designed in pusher configuration to allow unobstructed view for additional payload like camera. The plane was equipped with Cube V5+ autopilot running open-source plane firmware Arduplane v4.2.

Architecture of the autopilot and its peripheral are shown in figure 3.6:

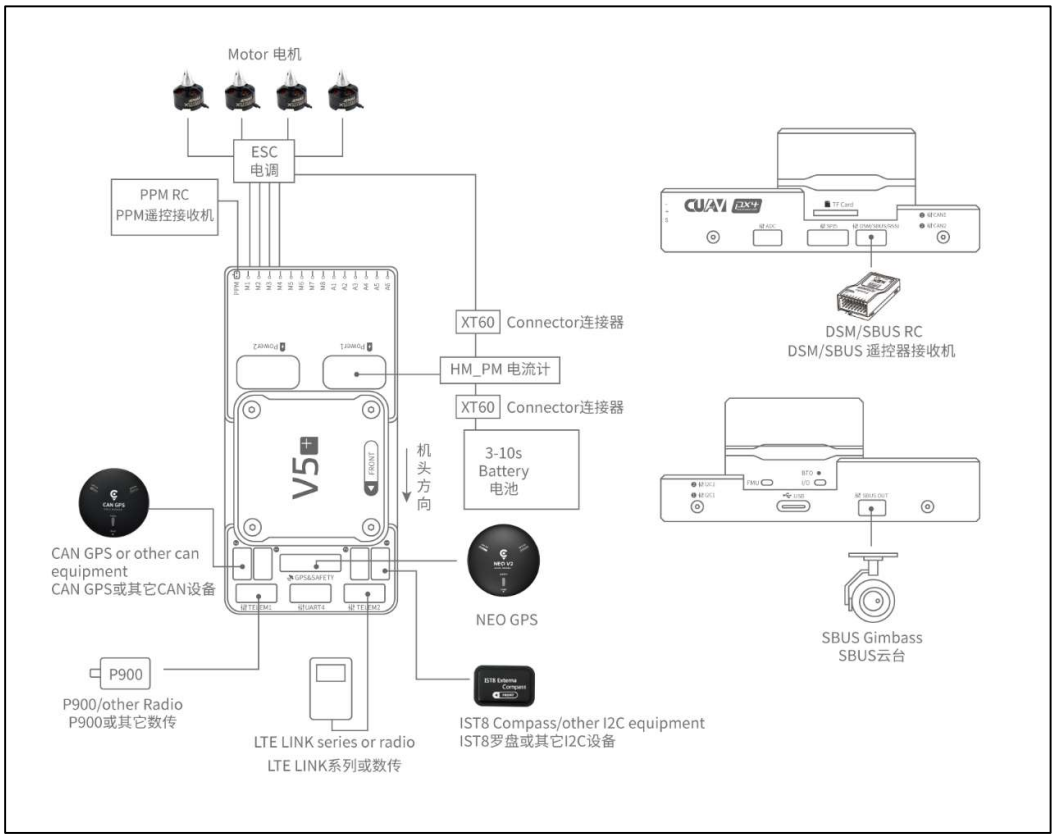

Fig 3.6: Architecture of the autopilot and its peripheral
(Source: www.cuav.net)

3.3.2 Ground Control Station

The Ground Control Station (GCS) of the UAV is composed of a laptop computer running open-source Mission Planner Software which serves as the controlling station of the UAV. In addition to that Mission Planner also provides an interface for loading mission profile, configuration of autopilot, calibration of sensors. It also provides tools for downloading and analyzing the flight logs to extract sensor data.

Fig 3.7: GCS Head Up Display (HUD)

Mission Planner connects to the autopilot by data link (MAVLINK protocol) hich was created using Microhard P900 data radio. It runs in 902 MHz-928 MHz ISM band and can provide data rate of 56 Kbps which is enough for the UAV to downstream its positions and attitude information as well as sensor data. The P900 radio provides an output 30 dB_m which if amplified using a 10 watt RF (40 dB_m) amplifier. A 6 dB gain dipole antenna is connected to ensure connectivity in direction.

A standard 16 channel radio controller is also used as the backup controller to take over the UAV manually in case of any emergency. The radio operates in 433 MHz ISM band with an output of 30 dB_m.

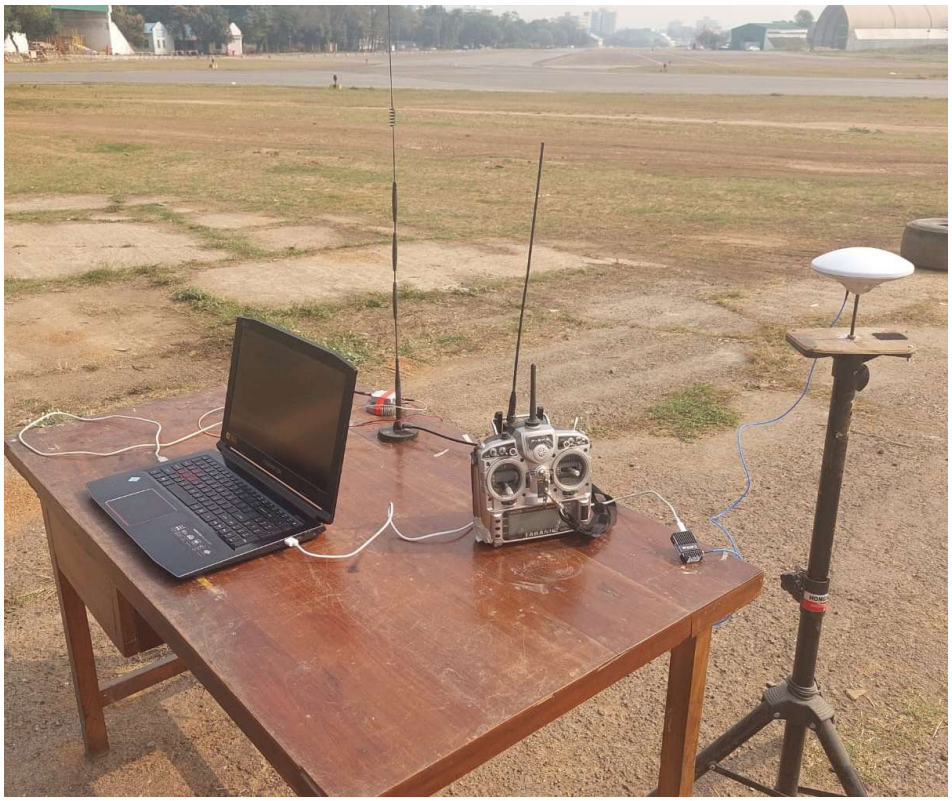

Fig 3.8: RTK GPS and GCS setup for Test Flight

Fig 3.9: The designed UAV for real test flight

3.3.3 RTK GPS Base Station

Accuracy of GPS can be increased by using Real Time Kinematics correctional data with the newer F9P generation of GPS. Propagation and timing corrections (RTCM data) for each satellite can be fed to the vehicle's RTK GPS in several ways:

a. From a local RTK base station connected to the GCS, which is also connected to the vehicle (via MAVLink)
b. By forwarding RTCM correction data from an NTRIP server via the internet connected GCS, which is also connected to the vehicle (via MAVLink)
c. Wirelessly from a local RTK base station directly to the vehicle GPS's secondary UART port

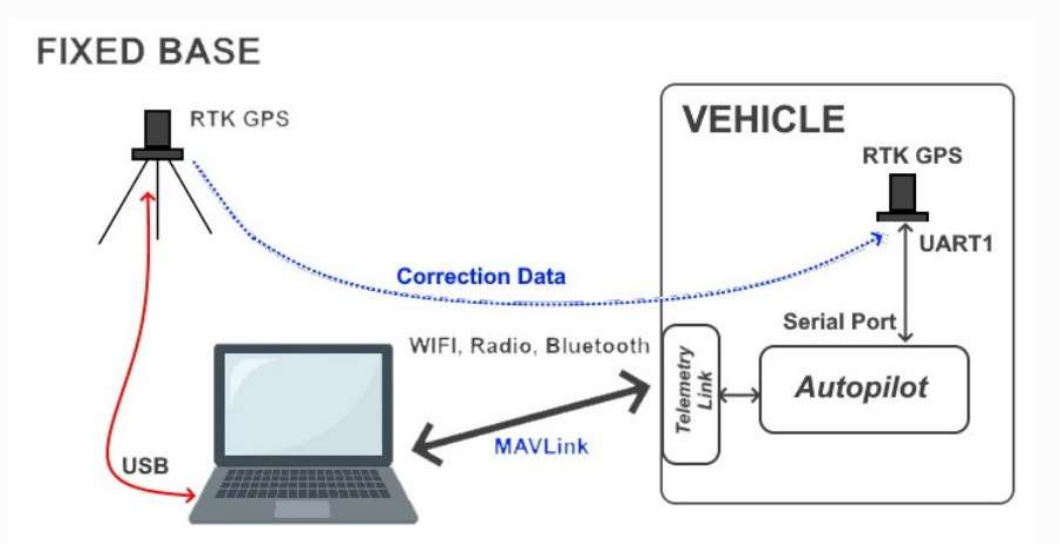

Fig 3.10: RTK augmentation signal transmission through Data Link
Source: www.ardupilot.org

For this investigation Fixed Base strategy has been used. In this setup, the correction data is passed from the Base unit through the GCS program to the vehicle's MAVLink connection to the GCS, providing the vehicle's RTK GPS with correction data to enable its position reporting to become more accurate.

This method requires that the RTK Base station's position be precisely known or determined. Usually, this requires that the GCS command the RTK Base GPS to "survey-

in" itself. The GPS takes many measurements determining its mean location, applying interim corrections, and continues to refine its location deviations until the measurements are within a set threshold of error (usually a few meters) for a given time period (usually 60 seconds). The GPS then uses that as its location and start outputting the correction data to the GCS for forwarding to the vehicle's GPS.

It is possible to program the RTK Base's exact location directly into it if it is known using the UBlox programming tool or Mission Planner if that location has been previously "surveyed-in".

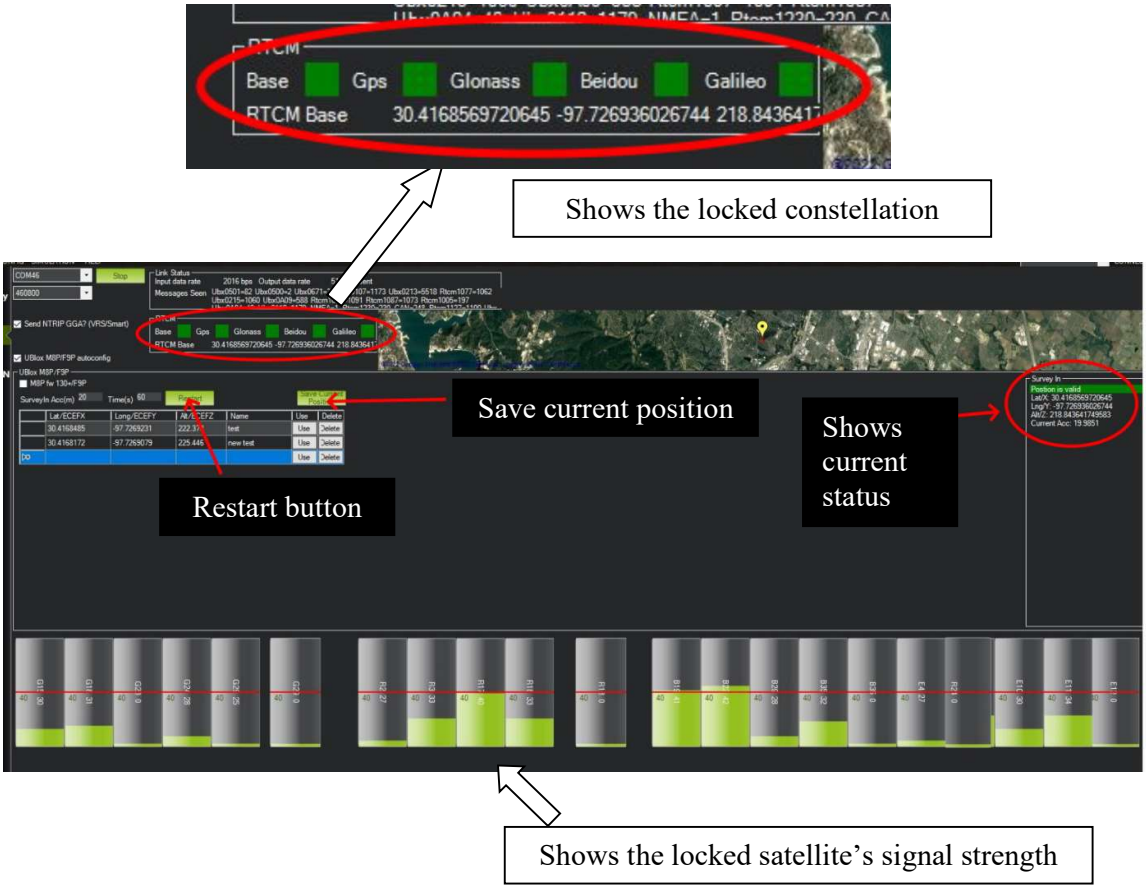

Fig 3.11: RTK Base GPS to "survey-in" procedure
Source: www.ardupilot.org

3.4 Mission profile

The aircraft was flown in a simple circuit pattern maintaining 60 m altitude. The full mission was planned on ground station on google map and was verified carefully to eliminate any discrepancy. The aircraft was flown in clam weather to minimize weather

effects as best as it can be. The same flight plan was repeatedly flown with different combinations altitude sensors.

3.4.1 Test Setup 1

As literature review reveals that vertical accuracy of GPS is not enough for precision flare, it was not used as landing aid sensor for the test flight. Although the UAV was equipped with GPS it was mainly used for navigation only. In addition to that RTK GPS and RTK base station were setup and Correction data from the RTK base was infused in the primary datalink to eliminate the need of additional radio. 5 test flight sorties were carried out using the same flight plan and in same type of weather as practicable.

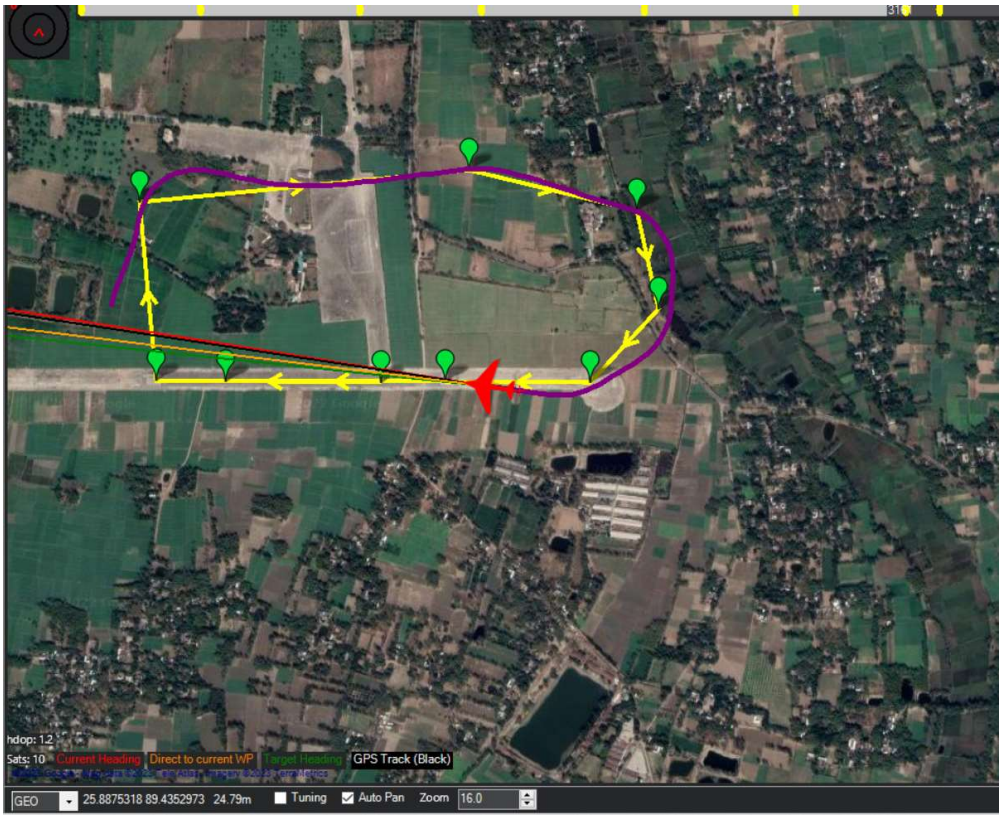

Fig 3.12: Flight Plan for the Test Flight

3.4.2 Test Setup 2

Same setup like setup 1 with an addition of Laser Range finder working as Laser altimeter. Laser Altimeter has been used as the primary source of altitude during the landing phase whereas RTK GPS has been used for navigation and source of altitude in

all phases except landing phase. 5 actual flight sorties have been carried out with same flight plan and in same type of weather.

3.5 Chapter Summary

In this chapter, a simulation setup has been discussed to analyze the performance of four sensors by installing them, one by one, in a fixed wing UAV. Simulation software architecture and simulation conditions were also discussed briefly. After that a detailed scheme for the simulation to test the performance of the sensors were discussed elaborately.

The subsequent sections discussed a test set up comprising of a small fixed wing UAV and its ground control station to test those sensors by test flights. Airframe of the test platform, its autopilot architecture, control and data link were also discussed elaborately. After that RTK GPS setup along with base station and integration scheme with the UAV system has been discussed. The chapter concluded with discussion of scheme for the test flights suitable for testing the sensor performance.

CHAPTER 4
RESULTS AND ANALYSIS

4.1 Introduction

Four altitude estimating sensor were selected by literature review and analysis in the previous chapters to be used as flare altitude estimating. Chapter 3 discussed the detailed scheme to test those sensors in simulation flights and test flights to find out the actual performance in landing phase. This chapter discusses in detail about the analysis method, statistical tool that has been used to analyze the results.

The subsequent sections of this chapter analyze the data obtained from simulation flights to find out best performing sensors in simulation. The selected sensors have been used in real test flight. The concluding section of this chapter discusses the data obtained from real test flights and compare the results with simulation.

4.2 Data extraction

After each test flight or simulation, the light log is downloaded from the autopilot and analyzed by using log analysis tool.

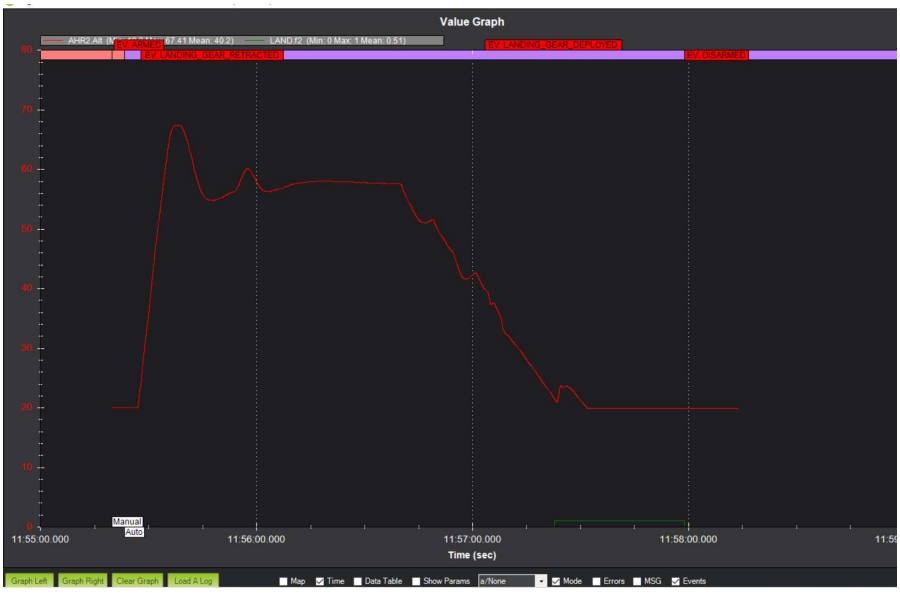

Fig: 4.1 Flight log showing the altitude AGL vs Time

Figure 4.1 shows the UAV altitude vs time in red line. At 11:57:22 the UAV starts the flare procedure and raises its attitude. Further zooming on to the curve in the flare phase (marked in green) revels the UAV altitude above calculated terrain altitude or Above Ground Level (AGL).

Fig 4.2: Altitude during Flare Phase and portion of flight path

Right side of the figure shows the position of the UAV on the Google map. Altitude at the starting of flare is $F_1 = 0.6$ m. Commanded flare altitude F_{Comd} was 1 m. so error in flare altitude F_{error}= 0.4 m.

4.3 Performance Comparison

Simulation mission profile has been kept simple which follows a circuit with 50 m maximum attitude with auto takeoff and landing following standard 3^0 glide slope. All the environmental variables like surface wind, temperature have been kept constant to obtain uniform simulation parameter. All the altitude measuring sensors under test like GPS, RTK GPS, Barometer, Range Finder were simulated one by one. For each sensor 75 simulations were carried out. The commanded altitude for the flare were selected as 1 m, 1.5 m and 2 m. For each commanded flare altitude, 25 simulations were carried out to check if there any variation of accuracy with commanded flare altitude. For all the error measurement, terrain data of Google Earth has been considered as reference. IBM

statistical tool SPSS has been used to analyze the results of total 300 simulations.

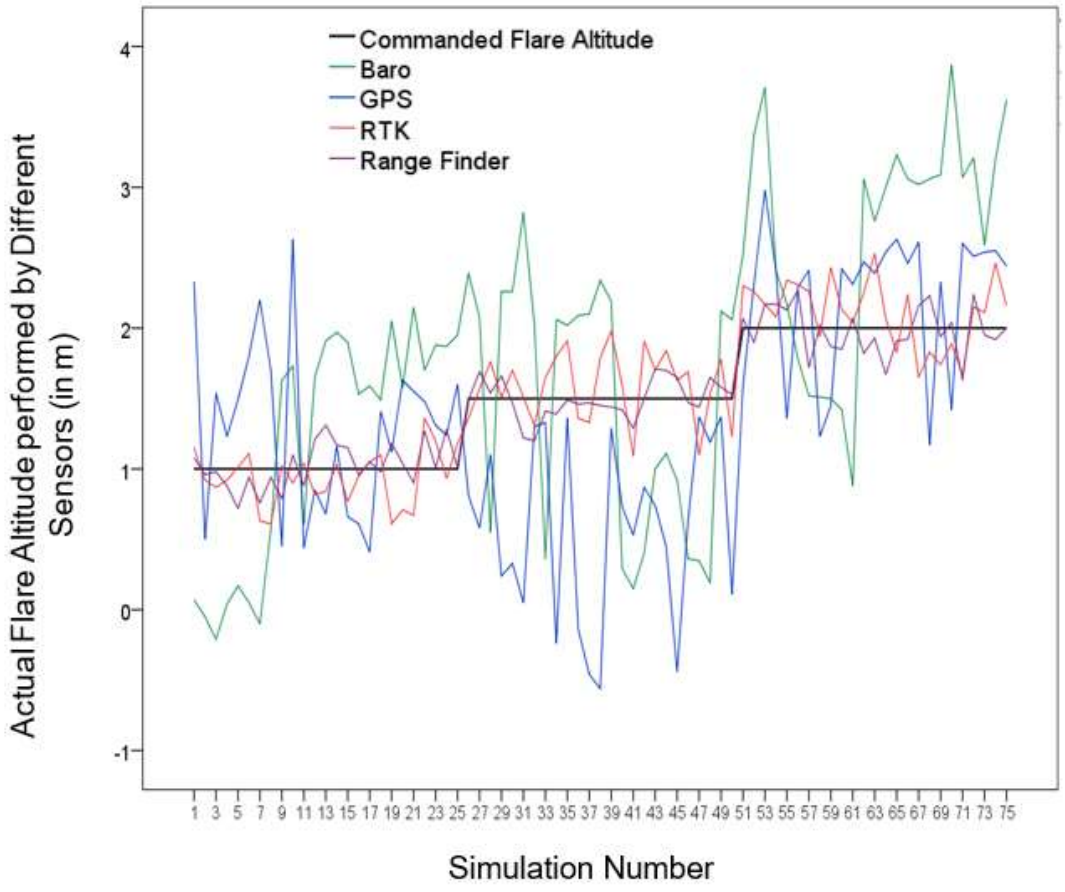

Fig 4.3: The graph shows actual performed flare altitude (represented by green, blue, red and purple line) against the commanded flare altitude (black line)

Figure 4.3 shows the actual flare altitude observed using different sensors against the commanded flare altitude. In all the cases (commanded and observed altitude), AGL altitude has been plotted in the graph. Fig 4.4 plots the error in flare altitude for each simulation result which is derived by subtracting commanded flare altitude from observed flare altitude (AGL).

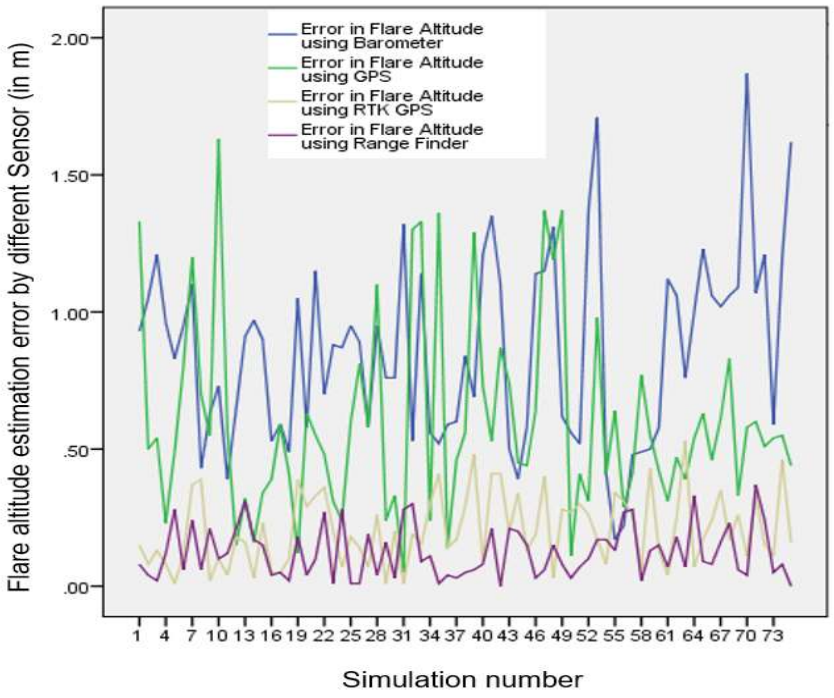

Fig 4.4: Error in estimating Flare Altitude by different sensors

Table 4.1. Error in Flare Altitude using different sensor

Sensor	Commanded Flare Altitude	Sim No	Mean	Std. Deviation	Min	Max
Barometer	1 m	25	0.8172	0.23109	0.39	1.21
	1.5 m	25	0.8256	0.30371	0.39	1.35
	2 m	25	0.9364	0.45255	0.17	1.87
	Total	75	0.8597	0.34154	0.17	1.87
GPS	1 m	25	0.5528	0.36510	0.12	1.63
	1.5 m	25	0.7292	0.44531	0.05	1.37
	2 m	25	0.5192	0.16713	0.29	0.98
	Total	75	0.6004	0.35384	0.05	1.63
RTK GPS	1 m	25	0.1640	0.12447	0.01	0.39
	1.5 m	25	0.2228	0.13480	0.01	0.48
	2 m	25	0.2296	0.13037	0.04	0.53
	Total	75	0.2055	0.13156	0.01	0.53
Range Finder	1 m	25	0.1268	0.09664	0.01	0.31
	1.5 m	25	0.1040	0.08723	0.00	0.30
	2 m	25	0.1416	0.09835	0.00	0.37
	Total	75	0.1241	0.09421	0.00	0.37

Table 4.2: Summary of Error in Flare Altitude using different sensor

Sensor	Sim No	Range (m)	Min (m)	Max (m)	Mean (m)	Std Deviation (m)
Barometer	75	1.70	0.17	1.87	0.86	0.34
GPS	75	1.58	0.05	1.63	0.60	0.35
RTK GPS	75	0.52	0.01	0.53	0.25	0.13
Range Finder	75	0.37	0.00	0.37	0.12	0.09

It has been observed that mean error from Barometer are 0.82 m, 0.83 m, 0.94 m for commanded flare altitude of 1 m, 1.5 m and 2 m respectively. Similarly, error from GPS for commanded altitude of 1 m, 1.5 m and 2 m has been observed as 0.55 m, 0.73 m and 0.52 m. Error from RTK GPS and Range Finder (LIDAR) for same set of commanded flare altitude have been found as 0.16 m, 0.22 m, 0.23 m and 0.13 m, 0.10 m, 0.14 m respectively.

To check if there is any variation of mean error with respect to commanded flare altitude, statistical tool Analysis of Variance (ANOVA) was used keeping the commanded flare altitude as independent variable and observed error as dependent variable. ANOVA is a well-known statistical tool that can be used for qualitative analysis of sensors by comparing sensors response to known control response [30]. For this investigation, two hypotheses have been assumed: H_0 = mean error of sensors for different flare altitude are same and H_1 = at least two of the means are not equal. If the value of Significance is smaller than 0.05, H_0 is rejected. Otherwise, evidence is insufficient to reject H_0 that means response of sensors (mean error) do not vary with changes of commanded flare altitude (considering 5% level of Significance) [31]. Table 4.3 shows result of ANOVA test.

Table 4.3: ANOVA on Simulation results

		Sum of Squares	df	Mean Square	F	Sig.
Error in Flare Altitude using Barometer	Between Groups	0.221	2	0.111	0.947	0.393
	Within Groups	8.411	72	0.117		
	Total	8.632	74			
Error in Flare Altitude using GPS	Between Groups	0.636	2	0.318	2.654	0.077
	Within Groups	8.629	72	0.120		
	Total	9.265	74			
Error in Flare Altitude using RTK GPS	Between Groups	0.065	2	0.033	1.926	0.153
	Within Groups	1.216	72	0.017		
	Total	1.281	74			
Error in Flare Altitude using Range Finder	Between Groups	0.018	2	0.009	1.011	0.369
	Within Groups	0.639	72	0.009		
	Total	0.657	74			

4.3.1 Barometric Altimeter

Average error in flare altitude using barometric altimeter has been found as 0.86 m with a standard deviation of 0.34 m. Error from barometric altimeter ranges from 0.17 m to 1.87 m. Mean error of 0.86 m ($\pm$0.34 m standard deviation) indicates that barometric altimeter will not be suitable for low level flare at 1m. Mean error for commanded flare altitude at 1m, 1.5 m and 2 m has been observed as 0.82 m, 0.83 m and 0.94 m respectively. Test result of ANOVA reveals that there is no statistically significant effect on mean error for different commanded flare altitude.

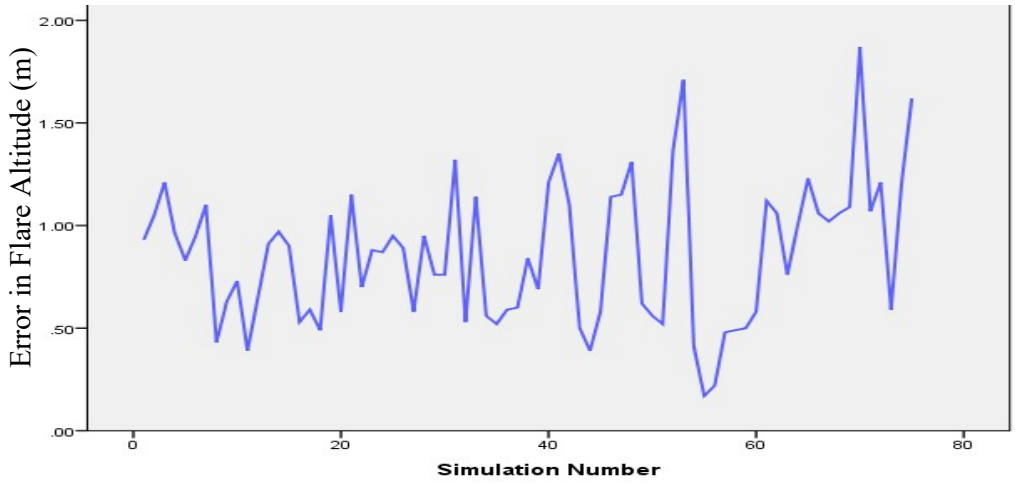

Fig 4.5: Error in Flare Altitude using Barometer

4.3.2 GPS

Average error in flare altitude using standard GPS as altitude sensor has been found as 0.60m with a standard deviation of 0.35 m. The mean error 0.60 m (±0.35 m standard deviation) indicates that standard GPS without any form of augmentation will not be suitable for low level flare at 1m. it also reveals that there is no statistically significant effect on mean error for different commanded flare altitude.

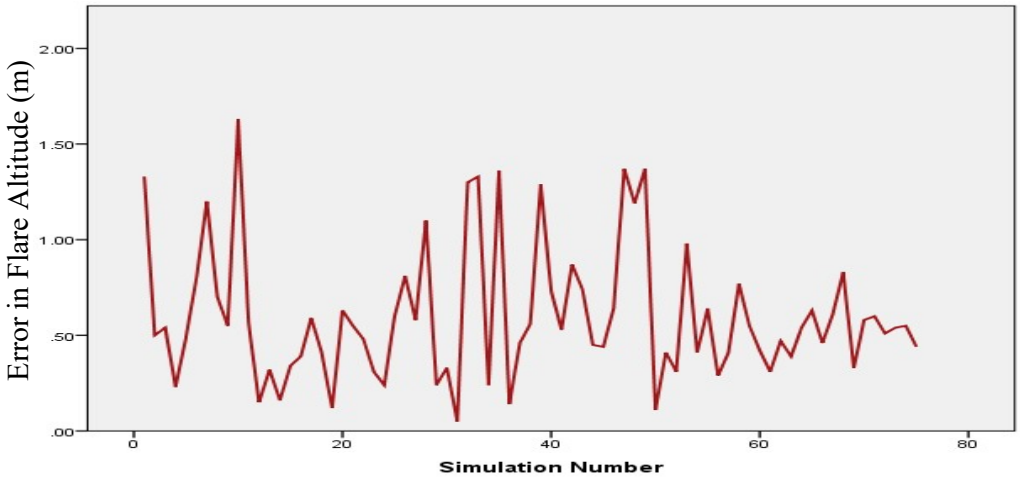

Fig 4.6: Error in Flare Altitude using GPS

4.3.3 RTK GPS

RTK GPS as altitude measuring sensor provides a mean error of 0.25 m (± 0.13 m standard deviation) while estimating flare altitude at different commanded

altitude. It also reveals that there is no statistically significant effect on mean error for different commanded flare altitude (value of significance 0.153).

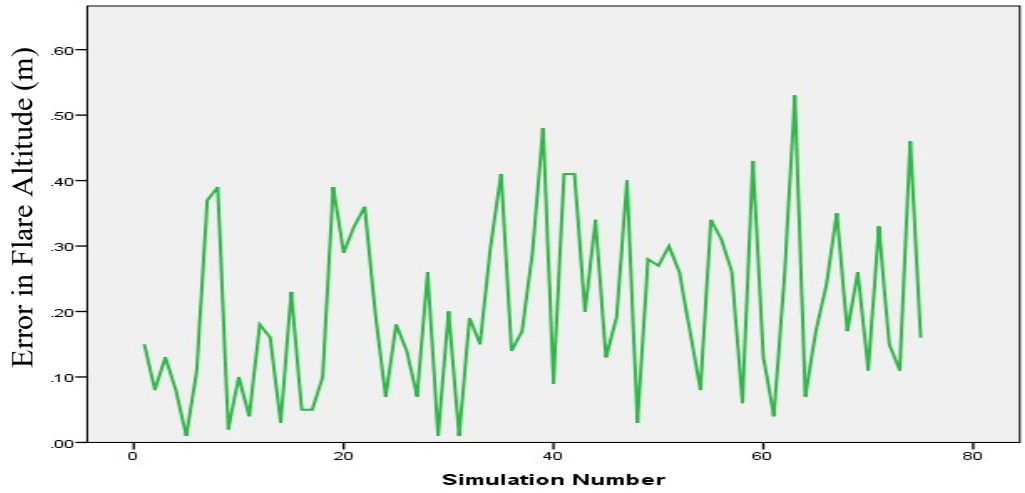

Fig 4.7: Error in Flare Altitude using RTK GPS

4.3.4 Laser Range Finder

Range finder (LIDAR) provided a mean error of 0.12m (± 0.09 m standard deviation) while estimating flare altitude at three different commanded altitude of 1 m, 1.5 m and 2 m.

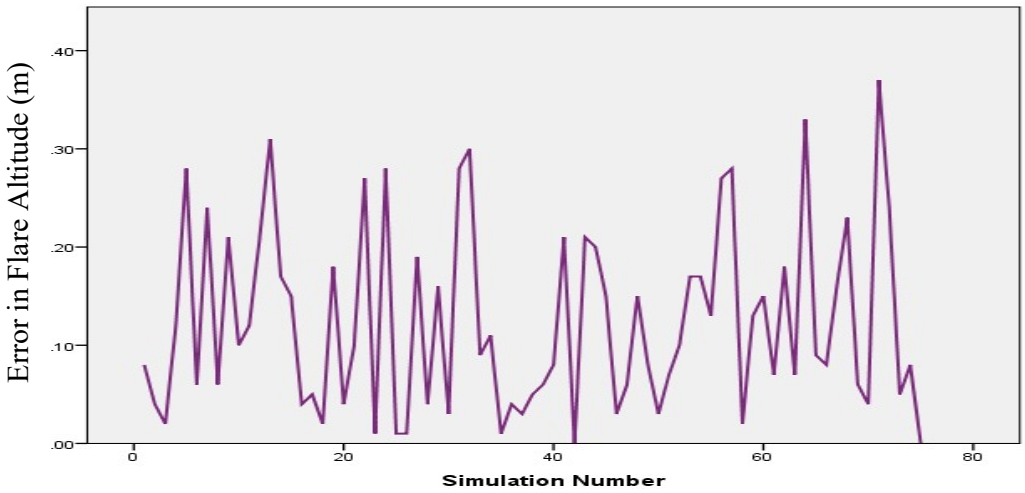

Fig 4.8: Error in Flare Altitude using Laser Range Finder

There is no statistically significant effect on mean error for different commanded flare altitude (value of significance 0.369).

4.4 Test Flight Results and Analysis

As discussed in the previous sections, simulation results show satisfactory performance from RTK GPS and LIDAR sensor. Average error obtained from RTK GPS is 0.25 m ($\pm$0.13 m standard deviation) against F_{comd}, whereas LIDAR estimated flare altitude with average error of 0.12m ($\pm$0.09m standard deviation) against F_{comd} of 1 m, 1.5 m and 2 m. Basing on the results, it was decided to test the performance of those two sensors in real test flight. As barometric altimeter performed with a mean error of 0.86 m ($\pm$0.34 m standard deviation) and GPS performed with mean error of mean error of 0.60 m (±0.35 m standard deviation) in simulation flights, those two sensors were not considered as flare altitude estimating sensor in real test flight. Accordingly, the UAV was fitted with RTK GPS and flown total 5 sorties. And after that, RTK GPS was replaced with LIDAR as altitude estimating senor for landing phase and again flown 05 sorties. In both the cases, standard GPS was fitted in the UAV but it was used only for navigation not during the landing phase. Data of GPS was also logged to compare the performance. Following graph shows the actual flaring altitude performed by the UAV with different sensors against the F_{comd}= 2 m (represented by the black line).

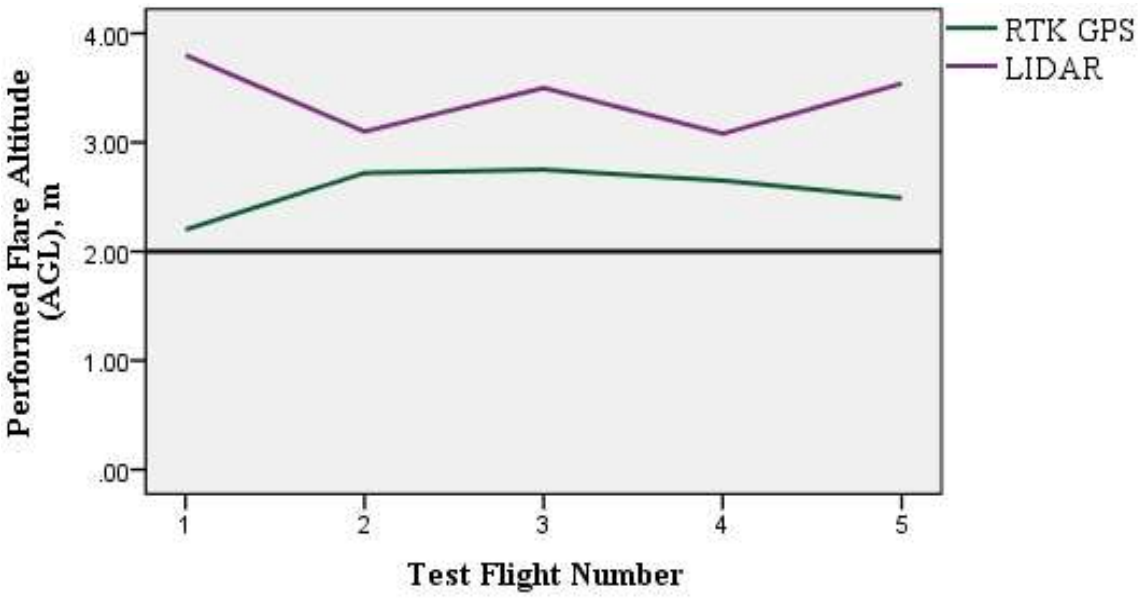

Fig 4.9: Performed Flare Altitude against commanded flare altitude (2 m)

In the test flights, autopilot behaved conservatively and performed flare above the F_{comd} altitude of 2 m. table 4.4 shows the summary of sensor performance in the test flights.

Table 4.4: Summary of Test Flight Results

	N	Range	Minimum	Maximum	Mean	Std. Deviation
Error in Flare Altitude using GPS	5	2.00	2.90	4.90	4.1600	0.79875
Error in Flare Altitude using RTK GPS	5	.55	0.20	0.75	.5620	0.22599
Error in Flare Altitude using Range Finder	5	1.26	0.54	1.80	1.2040	0.47695

Error in altitude estimation by RTK GPS ranges from 0.20 m to 0.75 m whereas error in altitude estimation by LIDAR ranges from 0.54 m to 1.80 m. Figure 4.10 shows the error in altitude estimation by those sensors:

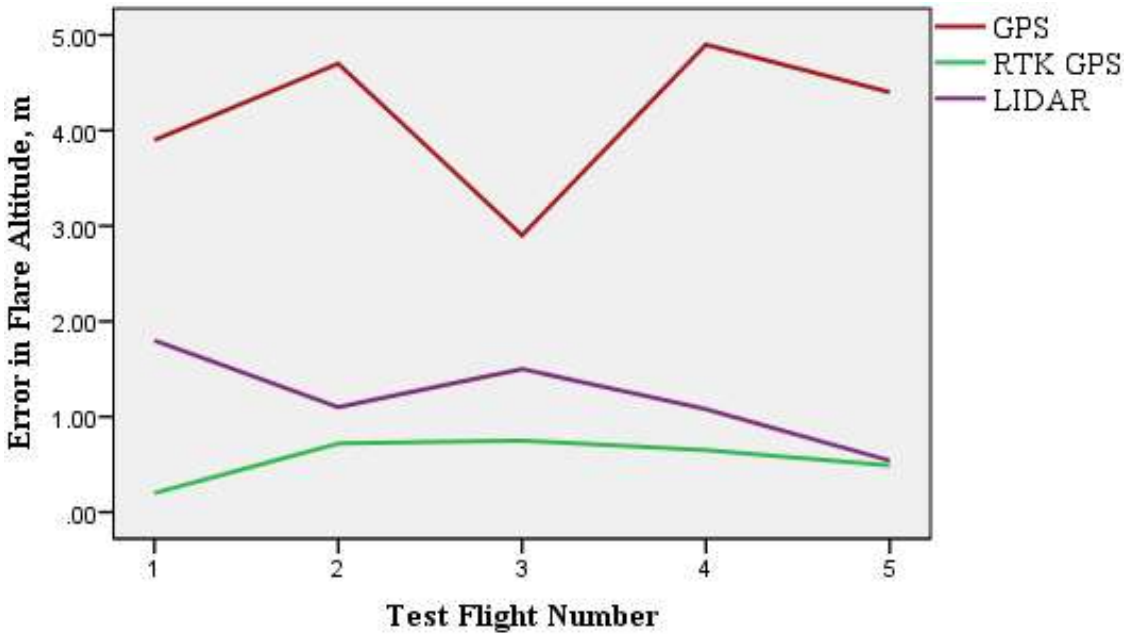

Fig 4.10: Comparison of error by different sensors

As there is considerably less number of flights compared to simulation and there was only one F_{comd} i.e 2m, ANOVA was not performed for test flight results.

4.4.1 Test Flight performance: RTK GPS

In 5 test flights, RTK GPS estimated flare altitude with a mean error of 0.56 m ($sd = \pm 0.23$ m) while estimating commanded flare attitude $F_{comd} = 2\ m$. During simulation flights RTK GPS estimated flare altitude with a mean error of 0.25 m (standard deviation $= \pm 0.13$ m).

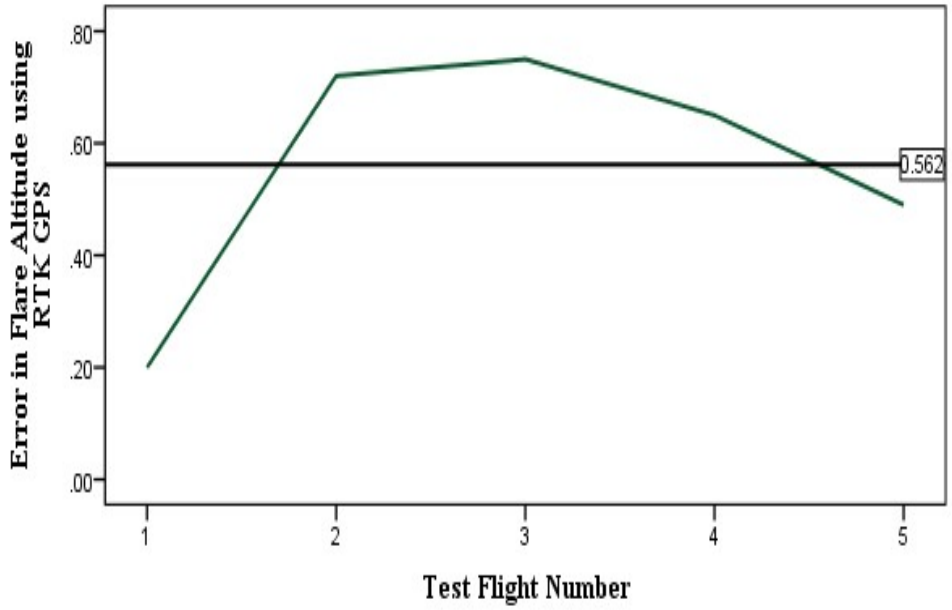

Fig 4.11: Error in flare altitude estimation by RTK GPS

Analyzing both results it can be said that RTK GPS performed consistently in both the cases while estimating vertical position (flare attitude).

4.4.2 Test Flight performance: LIDAR

In 5 test flights, LIDAR estimated flare altitude with a mean error of 1.20 m (standard deviation $= \pm 0.48$ m) while estimating commanded flare attitude $F_{comd} =$ 2 m. During simulation flights Laser Range Finder or LIDAR estimated flare altitude with a mean error of 0.12 m (standard deviation $= \pm 0.09$ m).

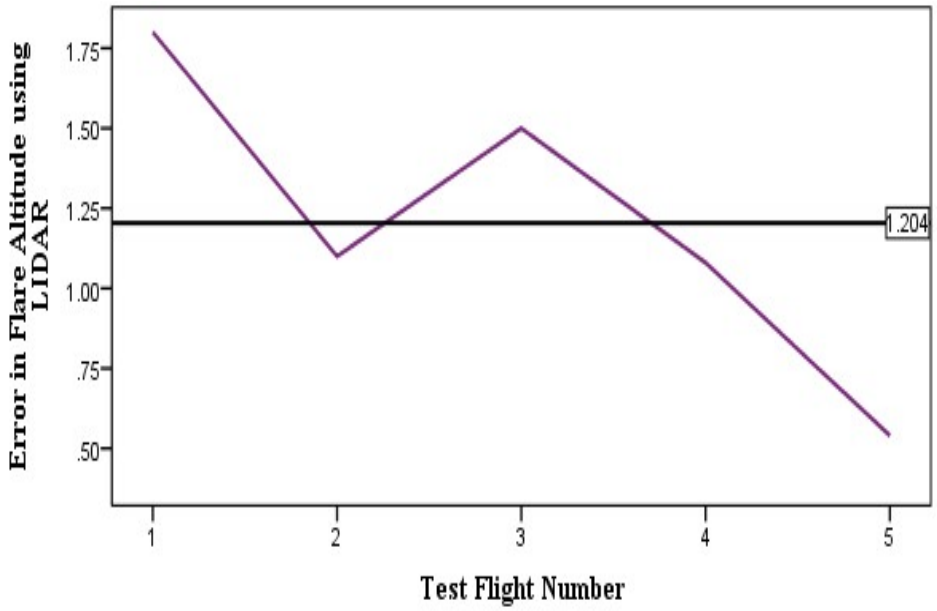

Fig 4.12: Error in flare altitude estimation by LIDAR sensor

During simulation flights, Laser Range Finder or LIDAR performed exceedingly good with exceptionally low error. However, during real test flights LIDAR performed satisfactorily with 1.2 m error. As commanded Flare altitude, F_{comd} has been set as 2 m, all the times the UAV flared at a higher altitude which resulted in longer floating time. But in all the cases the UAV touched down safely. The claimed accuracy of LIDAR sensor is 2.5 cm only whereas in real-time test flight the sensor performed with an error of 1.2 m. Environmental conditions like fog, uneven runway surface, variable wind speed and inherent aircraft factors of like autopilot pitch tunning, servo motor precision, calibration of autopilot are the main contributing factors of error in real test flight.

4.5 Chapter Summary

In this chapter, detailed analysis of the simulation flight results and real test flight results were analyzed. In simulations four sensors were tested one by one in total 300 simulations. Out of 75 simulations for each sensor, 25 simulations were carried out with different commanded flare altitude of 1 m,1.5 m and 2 m. In the simulations, LIDAR, RTK GPS, GPS and Barometer estimated flare altitude with an error of 0.12 m, 0.25 m, 0.6 m and 0.86 m respectively. Basing on the outcome of simulations two sensors i.e., RTK GPS and LIDAR were selected to be tested in real test flight.

In test flights, total 10 sorties of flight were carried out with 5 sorties for each sensor. Test flight result reveals that RTK GPS estimated flare altitude with a mean error of 0.56 m ($\text{standard deviation} = \pm 0.23$ m) whereas LIDAR sensor estimated flare altitude with a mean error of 1.20m ($sd = \pm 0.48$ m).

Both the sensor performed satisfactorily and could land the UAV safely. As estimated flare altitude was higher than the commanded flare altitude, the UAV floated for a longer time before touch down. Environmental conditions like fog, uneven runway surface, variable windspeed and aerodynamic factors like autopilot pitch tunning, precision of servo motor and calibration of autopilot are the main contributing factors of error in real test flight

CHAPTER 5
CONCLUSION

5.1 Conclusion

UAV system is a rapidly evolving technology that is becoming increasingly capable every day. UAV systems are expanding, augmenting and even replacing human efforts in civilian and military activities. Just like any other flights of manned aircraft, landing phase of fixed wing UAV is the most critical and challenging phase. This thesis is aimed at enhancing safety of autonomous landing of fixed wing UAV by analyzing the performance of few cost-effective sensors which can be utilized at altitude estimating sensor during the flare phase of landing.

Unfortunately, no literature is available matching the exact theme of this study. However, study conducted by [3] shows the performance of RTK GPS during net recovery of fixed wing UAV which estimated position with less than 1 m accuracy. For this investigation, four altitude estimating sensors i.e., RTK GPS, LIDAR, GPS and Barometer were selected for using them during the flare phase of landing. Testing of those sensors were done in two steps; in first step an open-source UAV simulator was used to test those sensors one by one. After analyzing the results of simulations, two sensors were selected to be tested in real test flights. All the flight logs were analyzed to evaluate the performance altitude estimating sensors during the flare phase of landing.

A simple simulation setup has been used to evaluate the performance of 4 inexpensive altitude measuring sensors during the flare phase of a fixed wing UAV. For each sensor, 75 simulations have been caried out with a grand total of 300 simulations for 4 sensors. Range finder (LIDAR) performed the best with mean error of 0.12 m while estimating flare altitude during landing. RTK GPS estimated altitude with 0.25 m mean error, while standard GPS and Barometric altimeter performed with mean error of 0.60 m and 0.86 m respectively which reveal that GPS and Barometric altimeter will not be suitable for low level flare at 1m during autonomous landing. No significant variation of error for different flare altitude has been observed. Based on the simulation results and cost, LIDAR rangefinder has been found as the most effective sensor whereas, RTK GPS has been found as the next best alternative for perfect and reliable flare altitude estimation. Basing on the outcome of simulations two sensors i.e., RTK GPS and LIDAR were selected to be tested in real test flight.

In test flights, total 10 sorties of flight were carried out with 5 sorties for each sensor. Test flight result reveals that RTK GPS estimated flare altitude with a mean error of 0.56 m (standard deviation $= \pm 0.23$ m) whereas, LIDAR sensor estimated flare altitude with a mean error of 1.20 m (standard deviation $= \pm 0.48$ m). Both the sensors performed satisfactorily and could land the UAV safely. As estimated flare altitude was higher than the commanded flare altitude, the UAV floated for a longer time before touch down. Environmental conditions like fog, uneven runway surface, variable windspeed and aerodynamic factors like autopilot pitch tunning, precision of servo motor and calibration of autopilot are the main contributing factors of error in real test flight

The simulation and test flight result validates the proof of concept of using low-cost sensors to estimate reliable flare altitude for fixed wing UAV.

5.2 Research Outcomes

With the pursuit of addressing the objectives, this research has contributed to a set of new findings that have been presented and published in the international conference proceedings. The complete results are also being drafted for possible publications in the reputable journals of related field. Proposed system of testing the sensors in this thesis thus captures the following major contributions to the UAV system and sensor research:

a. A new system has been proposed for evaluating the performance of altitude estimating sensors during the flare phase of fixed wing UAV.

b. During simulation, Range finder (LIDAR) performed the best with mean error of 0.12 m while estimating flare altitude during landing. RTK GPS estimated altitude with 0.25 m mean error, while standard GPS and Barometric altimeter performed with mean error of 0.60 m and 0.86 m respectively which reveal that standard GPS and Barometric altimeter will not be suitable for low level flare at 1m during autonomous landing.

c. There was no significant variation of error observed with change of commanded flare altitude.

d. Test flight result reveals that RTK GPS estimated flare altitude with a mean error of 0.56 m (standard deviation $= \pm 0.23$ m) whereas LIDAR sensor estimated flare altitude with a mean error of 1.20 m (standard deviation $= \pm 0.48$ m)

5.3 Significance of the research

As already mentioned above, this research contributes to the study of UAV sensor system. Notable significance of the thesis is stated below:

a. For the first time simulation and test flight setup has been proposed to evaluate the performance of altitude estimating sensors in the flare phase of fixed wing UAV.

b. Performance evaluation of altitude estimating sensors will certainly enhance flight safety of UAVs during landing phase.

c. Perfect altitude estimating sensor will eliminate the necessity of putting human in the loop during landing phase of UAV which will further enhance autonomy of UAVs.

d. Findings of this thesis i.e., performance evaluation of cost-effective sensor would reduce the overall cost of the UAV system

5.4 Future works

The findings presented in this thesis has also opened up a new direction in UAV system and sensor research to enhance flight safety and autonomy of UAV. Further research may be conducted the following directions:

a) Further improvement and perfection of the proposed testing scheme may be investigated considering the environmental and aerodynamic conditions.

b) Alternative sensors like optical flow sensor, sonar sensor, radar altimeter etc. may be investigated as landing aid sensor for fixed wing UAV.

c) Fusion of different sensors may be investigated to enhance the robustness of overall autonomous landing system.

PUBLICATIONS

Conference Paper

[1] M. M. Rahman and M. H.-E. Haider, "Performance Analysis of Effective Sensors for Determining Reliable Flare Altitude of Fixed Wing UAV," in *4th International Conference on Sustainable Technologies for Industry 4.0 (STI)*, Dhaka, 2022.

REFERENCES

[1] D. Klein, "Executive Summary of 2021 Defence Budget for Unmanned System and Robotics," AUVSI, 2023.

[2] Research and Markets, "Global UAV Market 2022-2026," 2022. [Online]. Available: https://www.researchandmarkets.com/reports/5229939/global-uav-market-2022-2026#relc0-5513572. [Accessed 02 03 2023].

[3] R. Skulstad, C. L. Syversen, M. Merz, N. Sokolova, T. I. Fossen and T. A. Johansen, "Net Recovery of UAV with Single-Frequency RTK GPS," in *2015 IEEE Aerospace Conference*, Big Sky, MT, USA, 2015.

[4] H. Yuxi, Z. Yi, C. Shuxiao and B. Mengyuan, "Research on UAV's Autonomous Target Landing with Image and GPS under Complex Environment," in *2019 International Conference on Communications, Information System and Computer Engineering (CISCE)*, Haikou, China, 2019.

[5] B. RONALD, "GPS III-Galileo/Altimeter Landing System for CAT IIIB: Concept and Analysis," *NAVIGATION: Journal of The Institute of Navigation,* vol. 55, no. 4, p. 267, 2008.

[6] D. Yasentsev, T. Shevgunov, E. Efimov and B. Tatarskiy, "Using Ground-Based Passive Reflectors for Improving," *MDPI,* 19 11 2021.

[7] P. Hügler, B. Driemeyer, T. Chaloun and C. Waldschmidt, "122 GHz Monostatic Radar Altimeter for Automated UAV Landing," in *International Conference on Electromagnetics in Advanced Applications (ICEAA)*, 2018.

[8] J. Jantawong and C. Deelertpaiboon, "Automatic Landing Control Based on GPS for Fixed- Wing Aircraft," in *15th International Conference on Electrical Engineering/Electronics, Computer, Telecommunications and Information Technology*, 2018.

[9] Y. Kang, B.-J. Park, A. Cho, C.-S. Yoo, Y. Kim, S. Choi, S.-O. Koo and S. Oh, "A

Precision Landing Test on Motion Platform and Shipboard of a Tilt-Rotor UAV Based on RTK-GNSS," *International Journal of Aeronautical and Space Sciences,* vol. 19, p. 994–1005, 22 September 2019.

[10] U. Papa, G. Ariante and G. D. Core, "UAS aided landing and obstacle detection throught LIDAR-Sonar data," in *5th IEEE International Workshop on Metrology for AeroSpace (MetroAeroSpace)*, Rome, Italy, 2018.

[11] F. Amzajerdian, G. D. Hines, V. E. Roback, L. B. Petway, B. W. Barnes and P. F. Brewster, "Advancing Lidar Sensors Technologies for Next Generation Landing Missions," in *AIAA Guidance, Navigation, and Control Conference*, 2015.

[12] F. Ahmed, J. C. Mohanta, A. Keshari and P. S. Yadav, "Recent Advances in Unmanned Aerial Vehicles: A Review," *Arabian Journal for Science and Engineering,* vol. 47, p. 7963–7984, 25 4 2022.

[13] Federal Aviation Authority, Airplane Flying Handbook, FAA-H-8083-3B ed., United States Department of Transportation, 2022.

[14] E. D. Kaplan and C. J. Hegarty, Understanding GPS/GNSS, Principles and Applications, 3 ed., Boston, London: Artech Houses, 2017, pp. 65-69.

[15] A. Kumar, S. Kumar, P. Lal, P. Saikia, P. K. Srivastava and G. P. Petropoulos, "Introduction to GPS/GNSS technology," in *GPS AND GNSS TECHNOLOGY IN GEOSCIENCES*, P. K. S. George P. Petropoulos, Ed., Elsevier, 2021, p. 15.

[16] A. Mauricio, "Real Time Kinematics RTK," [Online]. Available: http://mauricioandrada.medium.com/real-time-kinetics-rtk-dd791a8e55d5.

[17] W. Lambert, "Inroduction to Network RTK," IAG Working Group, 26 03 2021. [Online]. Available: http://www.wasoft.de/e/iagwg451/intro/introduction.html.

[18] H. Xu, "Application of GPS-RTK Technology in the Land Change Survey," *Procedia Engineering,* vol. 29, p. 3454 – 3459, 2012.

[19] S. Choy, "GNSS satellite-based augmentation systems for Australia," 29 9 2016. [Online]. Available: https://link.springer.com/article/10.1007/s10291-016-0569-

2#citeas.

[20] W. Tang, G. Howell and Y.-H. Tsai, "Barometric altimeter short-term accuracy analysis," *IEEE Aerospace and Electronic Systems Magazine,* vol. 20, no. 12, pp. 24-26, Dec 2005.

[21] Y. ZHAN, L. M. CHANG and J. LI, "Research of barometric altitude measurement technology," in *MATEC Web of Conferences 63:01014*, 2016.

[22] Federal Aviation Administration, "Title 14: Aeronautics and space," in *Rule by the Transportation Department, and the Federal Aviation Administration*, 2022.

[23] Measurement Specialties, Inc, *MS5611-01BA03,* TE Connectivity Ltd, 2017, p. 22.

[24] Garmin, "Garmin LIDAR-Lite v3 Optical Distance Measurement Sensor," Garmin, [Online]. Available: https://www.garmin.com/en-US/p/557294#specs. [Accessed 22 1 2022].

[25] W. Rees, Physical Principle of Remote Sensing, 3rd ed., Cambridge CB2 8RU, UK: Cambridge University Press, 2012.

[26] M. Kelemen, I. Virgala, T. Kelemenová, Ľ. Miková, P. Frankovský, T. Lipták and M. Lörinc, "Distance Measurement via Using of Ultrasonic Sensor," *Journal of Automation and Control,* vol. 3, no. 3, pp. 71-74, 2015.

[27] S. Wang, Q. Liu, S. Chen and Y. Xue, "Design and Application of Distance Measure Ultrasonic Sensor," in *Lecture Notes in Electrical Engineering*, vol. 178, Berlin, Springer, Berlin, Heidelberg, 2013, pp. 109-114.

[28] MaxBotix Incorporated, *I2CXL-MaxSonar High Performance Sonar Rangefinder Datasheet,* MaxBotix Inc, 2018.

[29] Ardupilot.org, "Software In The Loop Simulation," 2022. [Online]. Available: https://ardupilot.org/dev/docs/sitl-simulator-software-in-the-loop.html#sitl-simulator-software-in-the-loop. [Accessed 29 1 22].

[30] K. Johnston, K. Hutchenson, P. Nyffenegger and J. Cunningham, "Ensemble Sensor Inspection: ANOVA With Several-Independent Univariate Tests," *IEEE SENSORS*

JOURNAL, vol. 15, no. 1, pp. 19-26, 2015.

[31] R. E. Walpole, R. H. Myers, S. L. Myers and K. Ye, Probability & Statistics for Engineers & Scientists, 9th edition ed., Prentice Hall, 2012.

[32] M. M. Rahman and M. H.-E. Haider, "Performance Analysis of Effective Sensors for Determining Reliable Flare Altitude of Fixed Wing UAV," in *4th International Conference on Sustainable Technologies for Industry 4.0 (STI)*, Dhaka, 2022.

APPENDIX A

SIMULATION RESULTS FOR DIFFERENT SENSORS

SENSOR: GPS (1M)

SIM No	Commanded Flare Alt (m)	Terrain Height (m)	Actual Flare Alt (m)	Flare AGL (m)	Error (m)	Abs Error (m)
SIM-1	1	20.18	22.51	2.33	1.33	1.33
SIM-2	1	20.13	20.63	0.5	-0.5	0.5
SIM-3	1	20.11	21.65	1.54	0.54	0.54
SIM-4	1	19.3	20.53	1.23	0.23	0.23
SIM-5	1	20.19	21.68	1.49	0.49	0.49
SIM-6	1	20.08	21.88	1.8	0.8	0.8
SIM-7	1	20.18	22.38	2.2	1.2	1.2
SIM-8	1	20.19	21.89	1.7	0.7	0.7
SIM-9	1	20.28	20.73	0.45	-0.55	0.55
SIM-10	1	19.31	21.94	2.63	1.63	1.63
SIM-11	1	20.14	20.58	0.44	-0.56	0.56
SIM-12	1	20.2	21.05	0.85	-0.15	0.15
SIM-13	1	20.21	20.89	0.68	-0.32	0.32
SIM-14	1	20.05	21.21	1.16	0.16	0.16
SIM-15	1	20.16	20.82	0.66	-0.34	0.34
SIM-16	1	20.21	20.82	0.61	-0.39	0.39
SIM-17	1	20.22	20.63	0.41	-0.59	0.59
SIM-18	1	20.24	21.65	1.41	0.41	0.41
SIM-19	1	20.15	21.27	1.12	0.12	0.12
SIM-20	1	20.08	21.71	1.63	0.63	0.63
SIM-21	1	20.16	21.71	1.55	0.55	0.55
SIM-22	1	20.27	21.75	1.48	0.48	0.48
SIM-23	1	20.23	21.54	1.31	0.31	0.31
SIM-24	1	19.32	20.56	1.24	0.24	0.24
SIM-25	1	19.53	21.13	1.6	0.6	0.6

SENSOR: GPS (1.5M)

SIM No	Commanded Flare Alt (m)	Terrain Height (m)	Actual Flare Alt (m)	Flare AGL (m)	Error (m)	Abs Error (m)
SIM-1	1.5	19.96	22.27	2.31	0.81	0.81
SIM-2	1.5	20.01	22.09	2.08	0.58	0.58
SIM-3	1.5	19.45	22.05	2.6	1.1	1.1
SIM-4	1.5	20.05	21.79	1.74	0.24	0.24
SIM-5	1.5	19.95	21.78	1.83	0.33	0.33
SIM-6	1.5	20.05	21.6	1.55	0.05	0.05
SIM-7	1.5	19.96	22.76	2.8	1.3	1.3
SIM-8	1.5	20.01	22.84	2.83	1.33	1.33
SIM-9	1.5	21.81	23.07	1.26	-0.24	0.24
SIM-10	1.5	19.95	22.81	2.86	1.36	1.36
SIM-11	1.5	19.93	21.29	1.36	-0.14	0.14
SIM-12	1.5	19.92	20.96	1.04	-0.46	0.46
SIM-13	1.5	20.07	21.01	0.94	-0.56	0.56
SIM-14	1.5	19.99	22.78	2.79	1.29	1.29
SIM-15	1.5	19.87	22.1	2.23	0.73	0.73
SIM-16	1.5	19.97	22	2.03	0.53	0.53
SIM-17	1.5	19.96	22.33	2.37	0.87	0.87
SIM-18	1.5	20.06	22.3	2.24	0.74	0.74
SIM-19	1.5	19.91	21.86	1.95	0.45	0.45
SIM-20	1.5	19.98	21.04	1.06	-0.44	0.44
SIM-21	1.5	20.02	22.16	2.14	0.64	0.64
SIM-22	1.5	19.79	22.66	2.87	1.37	1.37
SIM-23	1.5	20.24	22.93	2.69	1.19	1.19
SIM-24	1.5	20.17	23.04	2.87	1.37	1.37
SIM-25	1.5	19.45	21.06	1.61	0.11	0.11

SENSOR: GPS (2M)

SIM No	Commanded Flare Alt (m)	Terrain Height (m)	Actual Flare Alt (m)	Flare AGL (m)	Error (m)	Abs Error (m)
SIM-1	2	20.12	21.71	1.59	-0.41	0.41
SIM-2	2	19.67	21.98	2.31	0.31	0.31
SIM-3	2	19.99	22.97	2.98	0.98	0.98
SIM-4	2	19.55	21.96	2.41	0.41	0.41
SIM-5	2	19.89	21.25	1.36	-0.64	0.64
SIM-6	2	19.67	21.96	2.29	0.29	0.29
SIM-7	2	19.55	21.96	2.41	0.41	0.41
SIM-8	2	19.96	21.19	1.23	-0.77	0.77
SIM-9	2	20.08	21.53	1.45	-0.55	0.55
SIM-10	2	19.64	22.06	2.42	0.42	0.42
SIM-11	2	19.67	21.98	2.31	0.31	0.31
SIM-12	2	19.54	22.01	2.47	0.47	0.47
SIM-13	2	19.88	22.27	2.39	0.39	0.39
SIM-14	2	19.64	22.18	2.54	0.54	0.54
SIM-15	2	19.76	22.39	2.63	0.63	0.63
SIM-16	2	19.82	22.28	2.46	0.46	0.46
SIM-17	2	19.77	22.38	2.61	0.61	0.61
SIM-18	2	20.21	21.38	1.17	-0.83	0.83
SIM-19	2	19.61	21.94	2.33	0.33	0.33
SIM-20	2	20.02	21.44	1.42	-0.58	0.58
SIM-21	2	19.69	22.29	2.6	0.6	0.6
SIM-22	2	19.78	22.29	2.51	0.51	0.51
SIM-23	2	19.71	22.25	2.54	0.54	0.54
SIM-24	2	19.7	22.25	2.55	0.55	0.55
SIM-25	2	19.85	22.29	2.44	0.44	0.44

SENSOR: RTK GPS (1M)

SIM No	Commanded Flare Alt (m)	Terrain Height (m)	Actual Flare Alt (m)	Flare AGL (m)	Error (m)	Abs Error (m)
SIM-1	1	20.14	21.29	1.15	0.15	0.15
SIM-2	1	20.15	21.07	0.92	-0.08	0.08
SIM-3	1	20.14	21.01	0.87	-0.13	0.13
SIM-4	1	20.07	20.99	0.92	-0.08	0.08
SIM-5	1	20.18	21.19	1.01	0.01	0.01
SIM-6	1	20.12	21.23	1.11	0.11	0.11
SIM-7	1	20.26	20.89	0.63	-0.37	0.37
SIM-8	1	20.21	20.82	0.61	-0.39	0.39
SIM-9	1	20.19	21.21	1.02	0.02	0.02
SIM-10	1	20.23	21.13	0.9	-0.1	0.1
SIM-11	1	20.11	21.15	1.04	0.04	0.04
SIM-12	1	20.14	20.96	0.82	-0.18	0.18
SIM-13	1	20.19	21.03	0.84	-0.16	0.16
SIM-14	1	20.13	21.16	1.03	0.03	0.03
SIM-15	1	20.15	20.92	0.77	-0.23	0.23
SIM-16	1	20.08	21.03	0.95	-0.05	0.05
SIM-17	1	20.09	21.14	1.05	0.05	0.05
SIM-18	1	20.2	21.3	1.1	0.1	0.1
SIM-19	1	20.18	20.79	0.61	-0.39	0.39
SIM-20	1	20.25	20.96	0.71	-0.29	0.29
SIM-21	1	20.26	20.93	0.67	-0.33	0.33
SIM-22	1	20.11	21.47	1.36	0.36	0.36
SIM-23	1	20.11	21.31	1.2	0.2	0.2
SIM-24	1	20.15	21.08	0.93	-0.07	0.07
SIM-25	1	20.01	21.19	1.18	0.18	0.18

SENSOR: RTK GPS (1.5M)

SIM No	Commanded Flare Alt (m)	Terrain Height (m)	Actual Flare Alt (m)	Flare AGL (m)	Error (m)	Abs Error (m)
SIM-1	1.5	19.99	21.35	1.36	-0.14	0.14
SIM-2	1.5	19.92	21.49	1.57	0.07	0.07
SIM-3	1.5	19.99	21.75	1.76	0.26	0.26
SIM-4	1.5	19.86	21.37	1.51	0.01	0.01
SIM-5	1.5	19.99	21.69	1.7	0.2	0.2
SIM-6	1.5	20.27	21.78	1.51	0.01	0.01
SIM-7	1.5	20.26	21.57	1.31	-0.19	0.19
SIM-8	1.5	19.96	21.61	1.65	0.15	0.15
SIM-9	1.5	19.92	21.72	1.8	0.3	0.3
SIM-10	1.5	19.48	21.39	1.91	0.41	0.41
SIM-11	1.5	20.14	21.5	1.36	-0.14	0.14
SIM-12	1.5	20.27	21.6	1.33	-0.17	0.17
SIM-13	1.5	19.51	21.3	1.79	0.29	0.29
SIM-14	1.5	19.56	21.54	1.98	0.48	0.48
SIM-15	1.5	20.1	21.69	1.59	0.09	0.09
SIM-16	1.5	20.22	21.31	1.09	-0.41	0.41
SIM-17	1.5	19.71	21.62	1.91	0.41	0.41
SIM-18	1.5	19.97	21.67	1.7	0.2	0.2
SIM-19	1.5	19.9	21.74	1.84	0.34	0.34
SIM-20	1.5	20	21.63	1.63	0.13	0.13
SIM-21	1.5	19.86	21.55	1.69	0.19	0.19
SIM-22	1.5	20.29	21.39	1.1	-0.4	0.4
SIM-23	1.5	20.09	21.62	1.53	0.03	0.03
SIM-24	1.5	20.04	21.82	1.78	0.28	0.28
SIM-25	1.5	20.09	21.32	1.23	-0.27	0.27

SENSOR: RTK GPS (2M)

SIM No	Commanded Flare Alt (m)	Terrain Height (m)	Actual Flare Alt (m)	Flare AGL (m)	Error (m)	Abs Error (m)
SIM-1	2	19.79	22.09	2.3	0.3	0.3
SIM-2	2	19.82	22.08	2.26	0.26	0.26
SIM-3	2	19.82	21.99	2.17	0.17	0.17
SIM-4	2	19.96	22.04	2.08	0.08	0.08
SIM-5	2	19.82	22.16	2.34	0.34	0.34
SIM-6	2	19.9	22.21	2.31	0.31	0.31
SIM-7	2	19.61	21.87	2.26	0.26	0.26
SIM-8	2	20.08	22.02	1.94	-0.06	0.06
SIM-9	2	19.68	22.11	2.43	0.43	0.43
SIM-10	2	20.02	22.15	2.13	0.13	0.13
SIM-11	2	19.87	21.91	2.04	0.04	0.04
SIM-12	2	19.59	21.84	2.25	0.25	0.25
SIM-13	2	19.68	22.21	2.53	0.53	0.53
SIM-14	2	20.17	22.24	2.07	0.07	0.07
SIM-15	2	20.23	22.06	1.83	-0.17	0.17
SIM-16	2	19.87	22.11	2.24	0.24	0.24
SIM-17	2	20.08	21.73	1.65	-0.35	0.35
SIM-18	2	20.15	21.98	1.83	-0.17	0.17
SIM-19	2	19.89	21.63	1.74	-0.26	0.26
SIM-20	2	19.79	21.68	1.89	-0.11	0.11
SIM-21	2	20.2	21.87	1.67	-0.33	0.33
SIM-22	2	19.92	22.07	2.15	0.15	0.15
SIM-23	2	19.96	22.07	2.11	0.11	0.11
SIM-24	2	19.91	22.37	2.46	0.46	0.46
SIM-25	2	19.83	21.99	2.16	0.16	0.16

SENSOR: BAROMETER (1M)

SIM No	Commanded Flare Alt (m)	Terrain Height (m)	Actual Flare Alt (m)	Flare AGL (m)	Error (m)	Abs Error (m)
SIM-1	1	20.13	20.2	0.07	-0.93	0.93
SIM-2	1	20.15	20.1	-0.05	-1.05	1.05
SIM-3	1	20.18	19.97	-0.21	-1.21	1.21
SIM-4	1	20.2	20.24	0.04	-0.96	0.96
SIM-5	1	20.1	20.27	0.17	-0.83	0.83
SIM-6	1	20.18	20.23	0.05	-0.95	0.95
SIM-7	1	20.1	20	-0.1	-1.1	1.1
SIM-8	1	21.16	21.73	0.57	-0.43	0.43
SIM-9	1	20.15	21.78	1.63	0.63	0.63
SIM-10	1	20.19	21.92	1.73	0.73	0.73
SIM-11	1	20.23	20.84	0.61	-0.39	0.39
SIM-12	1	20.14	21.79	1.65	0.65	0.65
SIM-13	1	20.13	22.04	1.91	0.91	0.91
SIM-14	1	20.04	22.01	1.97	0.97	0.97
SIM-15	1	20.08	21.98	1.9	0.9	0.9
SIM-16	1	20.23	21.76	1.53	0.53	0.53
SIM-17	1	20.14	21.73	1.59	0.59	0.59
SIM-18	1	20.07	21.56	1.49	0.49	0.49
SIM-19	1	20.07	22.12	2.05	1.05	1.05
SIM-20	1	20.15	21.73	1.58	0.58	0.58
SIM-21	1	20.04	22.19	2.15	1.15	1.15
SIM-22	1	20.11	21.81	1.7	0.7	0.7
SIM-23	1	20.22	22.1	1.88	0.88	0.88
SIM-24	1	20.19	22.06	1.87	0.87	0.87
SIM-25	1	20.14	22.09	1.95	0.95	0.95

SENSOR: BAROMETER (1.5M)

SIM No	Commanded Flare Alt (m)	Terrain Height (m)	Actual Flare Alt (m)	Flare AGL (m)	Error (m)	Abs Error (m)
SIM-1	1.5	20.01	22.4	2.39	0.89	0.89
SIM-2	1.5	20.01	22.09	2.08	0.58	0.58
SIM-3	1.5	19.81	20.36	0.55	-0.95	0.95
SIM-4	1.5	19.73	21.99	2.26	0.76	0.76
SIM-5	1.5	19.93	22.19	2.26	0.76	0.76
SIM-6	1.5	19.82	22.64	2.82	1.32	1.32
SIM-7	1.5	19.87	21.9	2.03	0.53	0.53
SIM-8	1.5	19.85	20.21	0.36	-1.14	1.14
SIM-9	1.5	20	22.06	2.06	0.56	0.56
SIM-10	1.5	20.01	22.03	2.02	0.52	0.52
SIM-11	1.5	19.97	22.06	2.09	0.59	0.59
SIM-12	1.5	20.1	22.2	2.1	0.6	0.6
SIM-13	1.5	20.01	22.35	2.34	0.84	0.84
SIM-14	1.5	20.01	22.2	2.19	0.69	0.69
SIM-15	1.5	20.04	20.33	0.29	-1.21	1.21
SIM-16	1.5	20.24	20.39	0.15	-1.35	1.35
SIM-17	1.5	19.93	20.33	0.4	-1.1	1.1
SIM-18	1.5	20.12	21.12	1	-0.5	0.5
SIM-19	1.5	19.93	21.04	1.11	-0.39	0.39
SIM-20	1.5	20.08	21	0.92	-0.58	0.58
SIM-21	1.5	20.01	20.37	0.36	-1.14	1.14
SIM-22	1.5	20.03	20.38	0.35	-1.15	1.15
SIM-23	1.5	20.16	20.35	0.19	-1.31	1.31
SIM-24	1.5	19.89	22.01	2.12	0.62	0.62
SIM-25	1.5	19.9	21.96	2.06	0.56	0.56

SENSOR: BAROMETER (2M)

SIM No	Commanded Flare Alt (m)	Terrain Height (m)	Actual Flare Alt (m)	Flare AGL (m)	Error (m)	Abs Error (m)
SIM-1	2	19.77	22.29	2.52	0.52	0.52
SIM-2	2	20.08	23.45	3.37	1.37	1.37
SIM-3	2	19.55	23.26	3.71	1.71	1.71
SIM-4	2	19.55	21.96	2.41	0.41	0.41
SIM-5	2	19.67	21.84	2.17	0.17	0.17
SIM-6	2	19.62	21.4	1.78	-0.22	0.22
SIM-7	2	19.71	21.23	1.52	-0.48	0.48
SIM-8	2	19.62	21.13	1.51	-0.49	0.49
SIM-9	2	19.68	21.18	1.5	-0.5	0.5
SIM-10	2	19.69	21.11	1.42	-0.58	0.58
SIM-11	2	20.24	21.12	0.88	-1.12	1.12
SIM-12	2	19.61	22.67	3.06	1.06	1.06
SIM-13	2	19.7	22.46	2.76	0.76	0.76
SIM-14	2	19.74	22.74	3	1	1
SIM-15	2	19.69	22.92	3.23	1.23	1.23
SIM-16	2	19.84	22.9	3.06	1.06	1.06
SIM-17	2	20.06	23.08	3.02	1.02	1.02
SIM-18	2	19.86	22.92	3.06	1.06	1.06
SIM-19	2	19.75	22.84	3.09	1.09	1.09
SIM-20	2	19.57	23.44	3.87	1.87	1.87
SIM-21	2	19.82	22.89	3.07	1.07	1.07
SIM-22	2	19.67	22.88	3.21	1.21	1.21
SIM-23	2	20.27	22.86	2.59	0.59	0.59
SIM-24	2	19.94	23.14	3.2	1.2	1.2
SIM-25	2	19.56	23.18	3.62	1.62	1.62

SENSOR: RANGE FINDER (1M)

SIM No	Commanded Flare Alt (m)	Terrain Height (m)	Actual Flare Alt (m)	Flare AGL (m)	Error (m)	Abs Error (m)
SIM-1	1	20.15	21.23	1.08	0.08	0.08
SIM-2	1	20.13	21.09	0.96	-0.04	0.04
SIM-3	1	20.23	21.21	0.98	-0.02	0.02
SIM-4	1	20.24	21.12	0.88	-0.12	0.12
SIM-5	1	20.13	20.85	0.72	-0.28	0.28
SIM-6	1	20.13	21.07	0.94	-0.06	0.06
SIM-7	1	20.23	20.99	0.76	-0.24	0.24
SIM-8	1	20.21	21.15	0.94	-0.06	0.06
SIM-9	1	20.11	20.9	0.79	-0.21	0.21
SIM-10	1	20.02	21.12	1.1	0.1	0.1
SIM-11	1	20.22	21.1	0.88	-0.12	0.12
SIM-12	1	20.15	21.36	1.21	0.21	0.21
SIM-13	1	20.12	21.43	1.31	0.31	0.31
SIM-14	1	20.19	21.36	1.17	0.17	0.17
SIM-15	1	20.23	21.38	1.15	0.15	0.15
SIM-16	1	20.19	21.15	0.96	-0.04	0.04
SIM-17	1	20.23	21.28	1.05	0.05	0.05
SIM-18	1	20.23	21.21	0.98	-0.02	0.02
SIM-19	1	20.15	21.33	1.18	0.18	0.18
SIM-20	1	20.13	21.17	1.04	0.04	0.04
SIM-21	1	20.21	21.11	0.9	-0.1	0.1
SIM-22	1	20.17	21.44	1.27	0.27	0.27
SIM-23	1	20.23	21.24	1.01	0.01	0.01
SIM-24	1	20.24	21.52	1.28	0.28	0.28
SIM-25	1	20.27	21.28	1.01	0.01	0.01

SENSOR: RANGE FINDER (1.5M)

SIM No	Commanded Flare Alt (m)	Terrain Height (m)	Actual Flare Alt (m)	Flare AGL (m)	Error (m)	Abs Error (m)
SIM-1	1.5	19.97	21.46	1.49	-0.01	0.01
SIM-2	1.5	19.95	21.64	1.69	0.19	0.19
SIM-3	1.5	19.95	21.49	1.54	0.04	0.04
SIM-4	1.5	19.82	21.48	1.66	0.16	0.16
SIM-5	1.5	20	21.47	1.47	-0.03	0.03
SIM-6	1.5	19.96	21.18	1.22	-0.28	0.28
SIM-7	1.5	19.97	21.17	1.2	-0.3	0.3
SIM-8	1.5	19.74	21.15	1.41	-0.09	0.09
SIM-9	1.5	19.99	21.38	1.39	-0.11	0.11
SIM-10	1.5	19.9	21.39	1.49	-0.01	0.01
SIM-11	1.5	19.93	21.39	1.46	-0.04	0.04
SIM-12	1.5	19.94	21.41	1.47	-0.03	0.03
SIM-13	1.5	19.81	21.26	1.45	-0.05	0.05
SIM-14	1.5	19.79	21.23	1.44	-0.06	0.06
SIM-15	1.5	19.93	21.35	1.42	-0.08	0.08
SIM-16	1.5	20.12	21.41	1.29	-0.21	0.21
SIM-17	1.5	20.01	21.51	1.5	0	0
SIM-18	1.5	19.98	21.69	1.71	0.21	0.21
SIM-19	1.5	19.95	21.65	1.7	0.2	0.2
SIM-20	1.5	19.96	21.61	1.65	0.15	0.15
SIM-21	1.5	19.87	21.34	1.47	-0.03	0.03
SIM-22	1.5	19.82	21.26	1.44	-0.06	0.06
SIM-23	1.5	19.88	21.53	1.65	0.15	0.15
SIM-24	1.5	19.83	21.41	1.58	0.08	0.08
SIM-25	1.5	19.98	21.51	1.53	0.03	0.03

SENSOR: RANGE FINDER (2M)

SIM No	Commanded Flare Alt (m)	Terrain Height (m)	Actual Flare Alt (m)	Flare AGL (m)	Error (m)	Abs Error (m)
SIM-1	2	19.56	21.63	2.07	0.07	0.07
SIM-2	2	19.56	21.46	1.9	-0.1	0.1
SIM-3	2	19.5	21.67	2.17	0.17	0.17
SIM-4	2	19.46	21.63	2.17	0.17	0.17
SIM-5	2	19.61	21.74	2.13	0.13	0.13
SIM-6	2	19.44	21.71	2.27	0.27	0.27
SIM-7	2	19.57	21.29	1.72	-0.28	0.28
SIM-8	2	19.5	21.52	2.02	0.02	0.02
SIM-9	2	19.4	21.27	1.87	-0.13	0.13
SIM-10	2	19.65	21.5	1.85	-0.15	0.15
SIM-11	2	19.52	21.59	2.07	0.07	0.07
SIM-12	2	19.43	21.25	1.82	-0.18	0.18
SIM-13	2	19.67	21.6	1.93	-0.07	0.07
SIM-14	2	19.52	21.19	1.67	-0.33	0.33
SIM-15	2	19.6	21.51	1.91	-0.09	0.09
SIM-16	2	19.67	21.59	1.92	-0.08	0.08
SIM-17	2	19.55	21.71	2.16	0.16	0.16
SIM-18	2	19.42	21.65	2.23	0.23	0.23
SIM-19	2	19.62	21.56	1.94	-0.06	0.06
SIM-20	2	19.62	21.66	2.04	0.04	0.04
SIM-21	2	19.87	21.5	1.63	-0.37	0.37
SIM-22	2	19.41	21.65	2.24	0.24	0.24
SIM-23	2	19.91	21.86	1.95	-0.05	0.05
SIM-24	2	19.69	21.61	1.92	-0.08	0.08
SIM-25	2	19.41	21.41	2	0	0

APPENDIX B
TEST FLIGHT RESULTS

GPS

Flight ID	Commanded Flare Alt (m)	Actual Flare, AGL (m)	Error (m)
1	2.0	5.90	3.90
2	2.0	6.70	4.70
3	2.0	4.90	2.90
4	2.0	6.90	4.90
5	2.0	6.40	4.40

RTK GPS

Flight ID	Commanded Flare Alt (m)	Actual Flare, AGL (m)_	Error (m)
1	2.0	2.20	0.20
2	2.0	2.72	0.72
3	2.0	2.75	0.75
4	2.0	2.65	0.65
5	2.0	2.49	0.49

LIDAR

Flight ID	Commanded Flare Alt (m)	Actual Flare, AGL (m)	Error (m)
6	2.0	3.80	1.80
7	2.0	3.10	1.10
8	2.0	3.50	1.50
9	2.0	3.08	1.08
10	2.0	3.54	.54